THE ATTENUATED RADON TRANSFORM: APPLICATION TO SINGLE-PHOTON EMISSION COMPUTED TOMOGRAPHY IN THE PRESENCE OF A VARIABLE ATTENUATING MEDIUM

Gullberg, Grant T.

1980-03-01

LBL-10276 c. 1
Preprint

Lawrence Berkeley Laboratory
UNIVERSITY OF CALIFORNIA

Submitted to SIAM Journal on Applied Mathematics

THE ATTENUATED RADON TRANSFORM: APPLICATION TO SINGLE-PHOTON EMISSION COMPUTED TOMOGRAPHY IN THE PRESENCE OF A VARIABLE ATTENUATING MEDIUM

Grant T. Gullberg

March 1980

tory
&
e
Division

Prepared for the U.S. Department of Energy under Contract W-7405-ENG-48

DISCLAIMER

LBL-10276

THE ATTENUATED RADON TRANSFORM: APPLICATION TO SINGLE-PHOTON EMISSION COMPUTED TOMOGRAPHY IN THE PRESENCE OF A VARIABLE ATTENUATING MEDIUM

GRANT T. GULLBERG

Donner Laboratory
Lawrence Berkeley Laboratory
University of California
Berkeley, California 94720

THE ATTENUATED RADON TRANSFORM: APPLICATION TO SINGLE-PHOTON EMISSION COMPUTED TOMOGRAPHY IN THE PRESENCE OF A VARIABLE ATTENUATING MEDIUM

Table of Contents

THE ATTENUATED RADON TRANSFORM: APPLICATION TO SINGLE-PHOTON EMISSION COMPUTED TOMOGRAPHY IN THE PRESENCE OF A VARIABLE ATTENUATING MEDIUM

Grant T. Gullberg

Donner Laboratory
Lawrence Berkeley Laboratory
University of California
Berkeley, California 94720

ABSTRACT

The properties of the attenuated Radon transform and its application to single-photon emission computed tomography (ECT) are analyzed in detail. In nuclear medicine and biological research, the objective of ECT is to describe quantitatively the position and strengths of internal sources of injected radiopharmaceuticals and radionuclides where the attenuation between the sources and detector is unknown. The problem is mathematically and practically quite different from well-known methods in transmission computed tomography (TCT) where only the attenuation is unknown. A mathematical structure using function theory and the theory of linear operators on Hilbert spaces is developed to better understand the spectral properties of the attenuated Radon transform. The continuous attenuated Radon transform is reduced to a matrix operator for discrete angular and lateral sampling, and the reconstruction problem reduces to a system of linear equations. For variable attenuation coefficients frequently found in imaging internal organs, the numerical methods developed in this paper involve iterative techniques of performing the generalized inverse. Its application to nuclear medicine is demonstrated by reconstructions of transverse sections of the brain, heart, and liver.

1. Introduction. The attenuated Radon transform describes mathematically the relationship between the number of photons emitted from radionuclide distributed in a transverse section of the body and the number of photons projected onto a scintillation detector [13]. Reconstruction procedures which numerically invert the attenuated Radon transform are used in single-photon emission computed tomography (ECT) to quantitate the three-dimensional distribution of gamma-emitting radiopharmaceuticals and radionuclides in the body. This application of ECT gives the physician a more accurate way of seeing inside the human body and provides a noninvasive procedure for studying biological processes both in health and in disease.

ECT is a field of nuclear medicine which uses projections of radionuclide distribution data — collected using scintillation detectors at different angles — to reconstruct cross-sectional images of the internal organs of the body. The instrumentation and strategies of ECT are divided into two major categories — 1) single-photon ECT, which uses either multiple-detector arrays [23],[45],[66] or scintillation cameras [4],[11], [39],[43] for the detection of single-photon emitting radionuclides such as ^{99m}Tc, and ^{123}I; and 2) positron ECT, which uses coincidence detection [8],[18],[57],[70] of annihilation photons from positron-emitting radionuclides such as ^{11}C, ^{13}N, ^{15}O, ^{68}Ga, and ^{82}Rb. In this paper we will be concerned with the former.

The major use of ECT is the quantitative *in vivo* measurement of biochemical and hemodynamic functions. This is in contrast to x-ray transmission computed tomography (TCT), which has as its major use the anatomic description of cross sections of body organs. The methods differ in principle: ECT seeks to describe the location and intensity of sources of emitted photons in an attenuating medium, whereas TCT seeks to determine the density distribution of the attenuating medium from the projected shadow of an external x-ray or gamma-ray emitting source. Single-photon ECT as exemplified by the attenuated Radon transform differs from both TCT and positron ECT in the mathematical procedures required to reconstruct the cross-sectional images. The attenuation compensation needed for single-photon ECT is not a simple multiplicative correction of the observed projection data as in the case of positron emission tomography [28]. However, iterative methods can be developed which adequately quantitate the distribution of single-photon radionuclides despite the attenuation of their radiation by a variable attenuation distribution.

The first clinically useful x-ray TCT machine was invented by Hounsfield of EMI, Ltd. in 1970 [35]. Since that time x-ray TCT has made a major impact on diagnostic radiological procedures with mathematical techniques and algorithms playing a central role [62],[64]. Even before the EMI scanner, the principles of ECT were worked out by Kuhl and Edwards [44]. However, the clinical application of ECT has lagged far behind that of x-ray TCT, primarily because the attenuation problem has made it difficult to quantitate the distribution of radionuclides. In the last 15 years, researchers have investigated different ways of reconstructing radionuclide distributions by developing new instruments and algorithms for inverting the attenuated Radon transform. These advances are reviewed in [9],[14],[28],[56],[69].

To illustrate the concepts of single-photon ECT, consider the example of a physician who is trying to detect small lesions in a patient's liver

(Fig. 1). The patient is injected with a radiopharmaceutical such as ^{99m}Tc sulfur colloid which localizes by phagocytosis in the Kupffer cells of the liver and other cells of the reticuloendothelial system. Cancer invasion results in failure of the diseased area to concentrate the colloidal particles [19].

A scintillation camera [1] — either fixed, with the patient rotating as illustrated in Fig. 2, or the with camera itself rotated by a gantry [43] — or a circular arrangement of scintillation detectors which scan in angle and horizontally [66] can be used to detect the photons emitted by the radionuclide ^{99m}Tc. The scintillation detector consists of a crystal which converts the high-energy gamma photons into light, and photomultiplier tubes which convert the light scintillation into an electronic signal. By electronic circuitry these electrical signals are used to display an image on an oscilloscope or are converted from analog to digital signals and stored in a computer for display as a digital image.

The images, commonly referred to as scintigrams, show an intensity directly proportional to the concentration of the radiopharmaceutical. Therefore a neoplastic lesion in the liver should show up on the images as a low intensity region surrounded by higher intensity from the normally functioning tissue. However, since the images represent the projection of the liver, overlying and underlying tissues, and other organs such as the spleen, the image of small lesions will be obliterated by the projection of these surrounding tissues onto the image plane.

To better visualize the liver and the suspected lesions, we obtain images at different angles, in which the internal organs appear in different relationships to one another. The information from a cross-

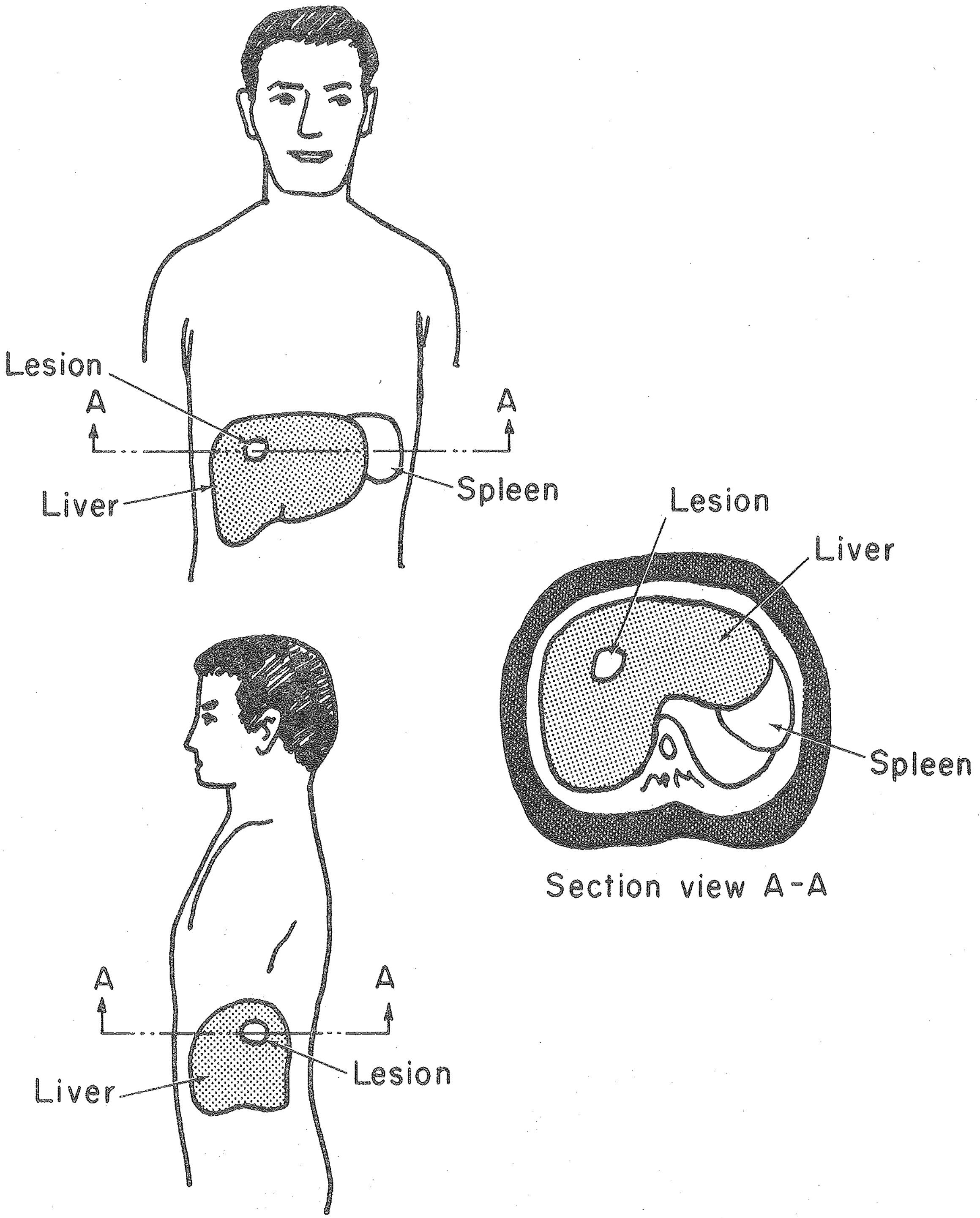

XBL7812-12398

Fig. 1. Illustration of a transverse section through the liver and spleen as one would view it looking from the feet toward the head. The anterior and left lateral views show the projected image of the lesion shown in the transverse section.

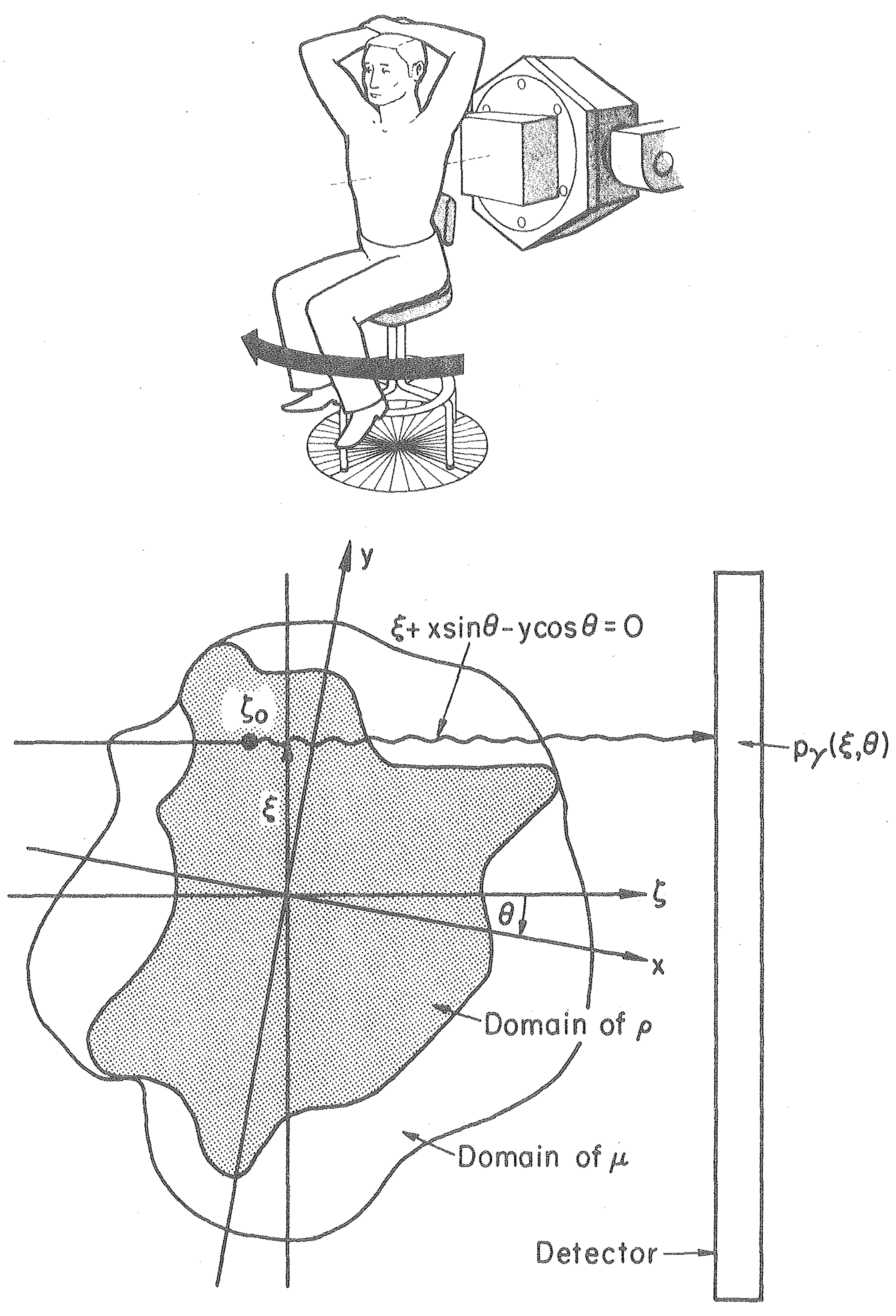

XBL7812-12396

Fig. 2. Single-photon emission computed tomography. At the rotation angle θ and lateral sampling ξ, the detector will see those photons which travel along the line $\xi + x\sin\theta - y\cos\theta = 0$ and are not attenuated by body tissue.

section of the body through the liver is recorded as a single one-dimensional line on each image. Taking this line for each angle and digitally processing the data, we reconstruct the desired two-dimensional cross section. This procedure separates the overlying and underlying tissue and allows the physician to quantitate the spatial distribution of the sulfur colloid sequestered by the liver. Lesions such as the one shown in Fig. 1 can be detected with better resolution and greater contrast than is possible with any of the traditional projected scintigrams.

The reconstruction of the cross-sectional image is complicated by the attenuation of the emitted photons. The scintillation detector can detect only those unattenuated photons projected along rays intersecting the camera face. The degree to which these photons are attenuated depends on the energy of the emitted photons and the density of the tissue interposed between the emitting source and the detector. For example, 78% of the 140 keV photons emitted from ^{99m}Tc radionuclides will be scattered or absorbed in passing through 10 cm of tissue. Therefore only 22% of these emitted photons will carry useful information. This presents a difficult problem for quantitating the actual distribution in any cross sectional image.

If mathematical algorithms appropriate for TCT [7],[25],[33],[38],[59],[63] are applied to projection data obtained from a scintillation camera, the results of reconstructing a uniform source within an attenuating medium such as the body will show a concentration which appears to be less in the center than at the edges. However, knowing the attenuation distribution, we can correct the effects of attenuation and obtain a true quantitative measure of the radionuclide concentration. The attenuation distribution is determined by TCT, using an external transmission source with the same energy as the emitted photon of the radionuclide (140 keV for ^{99m}Tc). The intensity of the transmitted beam is measured at different angles. These data are compared to the incident beam intensity and the results give a measure of the attenuation of the photons by the tissue between the source and the detector. The distribution of attenuation coefficients is reconstructed for the same cross sections as those chosen for the radionuclide cross-sectional images. With this *a priori* information about the character of the attenuating medium, we can use single-photon ECT to determine the location and intensity of the source of emitted photons by inverting the attenuated Radon transform.

To describe mathematically the single-photon ECT problem, we use ρ to denote the concentration of the radionuclide in counts/area at the point $\underset{\sim}{r} = (x,y)$, μ to denote the distribution of attenuation coefficients in units of $(\text{length})^{-1}$, and p to denote the projection of the emitted photons as illustrated in Fig. 2. The projections for a particular transverse section represent photons which have been released by radioactive nuclei that lie in the transverse section perpendicular to the detector. The photons measured are only those photons which are released within a solid angle subtended by the detector and collimator which are not attenuated by the body tissue between the nucleus and the detector. If a photon is emitted from a nucleus at the point ζ_0 and travels along the line $\xi + x \sin\theta - y \cos\theta = 0$, the probability that the photon will reach the detector is given by the formula

$$(1.1) \qquad \text{probability of photon escaping} = \exp\left[-\int_{\zeta \geqslant \zeta_0} \mu(\zeta,\xi,\theta)\,d\zeta\right] ,$$

where the distribution of attenuation coefficients μ is a function of tissue density and photon energy. The projection $p(\xi,\theta)$ at the angle θ and lateral sampling ξ is the line integral of ρ weighted by the exponential factor in (1.1):

$$(1.2) \qquad p(\xi,\theta) = \int \rho(\underset{\sim}{r}) \exp\left[- \int_{<\underset{\sim}{r}',\underset{\sim}{\theta}^{\perp}> \geqslant <\underset{\sim}{r},\underset{\sim}{\theta}^{\perp}>} \mu(\underset{\sim}{r}')\delta(\xi - <\underset{\sim}{r}',\underset{\sim}{\theta}>)d\underset{\sim}{r}'\right] \delta(\xi - <\underset{\sim}{r},\underset{\sim}{\theta}>)d\underset{\sim}{r} ,$$

where $\underset{\sim}{\theta} = (-\sin\theta,\cos\theta)$ and $\underset{\sim}{\theta}^{\perp} = (\cos\theta,\sin\theta)$. The mapping $A_{\mu}:\rho \to p$ in (1.2) is the attenuated Radon transform. If $\mu = 0$ everywhere, the attenuated Radon transform reduces to the transform [22], [48] defined by Radon in 1917 [58]. To define the attenuated Radon transform, the distribution of attenuation coefficients μ for the cross section is required. In some situations this distribution can be assumed to be constant, but for precise measurements it requires the use of TCT. The exponential term in (1.2) has, unfortunately, such large values for all energies used in nuclear medicine that the reconstructed images are seriously affected using TCT algorithms without compensating for attenuation.

This paper presents an analysis of the attenuated Radon transform and describes a reconstruction algorithm which uses an iterative method to numerically invert the attenuated Radon transform. The work presented differs from previous work in the literature [3],[4],[16],[36],[53],[71], [72] in that the attenuated Radon transform is defined for variable distributions of attenuation coefficients. Following this introduction, preliminary mathematical definitions and concepts are given which are used to formulate the properties of the attenuated Radon transform for both discrete angular sampling and continuous angular sampling. Then some basic theorems are given for the single-angle attenuated projection operator which maps L^2 spaces with special weight functions into L^2 spaces. These results are then extended to the continuous angle case. The generalized inverse and the singular value decomposition of compact operators are described in the context of the continuous angle operator. This gives a structure for the analysis of the mathematical and spectral properties of the attenuated Radon transform. The last two sections deal with iterative methods for inverting the attenuated Radon transform for arbitrary attenuation distributions, and with results obtained from patient and animal studies.

2. Preliminary definitions. The definition of the attenuated Radon transform A_μ given by (1.2) can be rewritten using the rotated coordinates (see Fig. 2):

$$\begin{aligned} x &= -\xi \sin\theta + \zeta \cos\theta \\ y &= \xi \cos\theta + \zeta \sin\theta \quad . \end{aligned} \tag{2.1}$$

This gives

$$p(\xi,\theta) = \int_{-\infty}^{\infty} \rho\left(-\xi \sin\theta + \zeta \cos\theta,\ \xi \cos\theta + \zeta \sin\theta\right) a(\zeta,\xi,\theta) d\zeta \ , \tag{2.2}$$

where

$$a(\zeta,\xi,\theta) = \exp\left[-\int_{\zeta}^{\infty} \mu(-\xi \sin\theta + \zeta' \cos\theta,\ \xi \cos\theta + \zeta' \sin\theta) d\zeta'\right] \quad . \tag{2.3}$$

The upper limit is chosen to be at infinity for mathematical convenience. This allows for general distributions of both concentration and attenuation coefficients; in practical situations, it does not matter if conceptually the detector is placed at infinity since the distribution of isotope concentration and attenuation coefficients is zero outside a compact subset of $\mathbb{R}^2$.

The distribution function ρ is a real valued function of the vector $\underset{\sim}{r}$. We will use the vector $\underset{\sim}{r}$ with coordinates (x,y) to denote the spatial position in the transverse section which has concentration density $\rho(\underset{\sim}{r})$. In (2.2) we see that the function ρ is mapped into the function $A_\mu \rho : \mathbb{C} = \mathbb{R} \times [0,2\pi) \to \mathbb{R}$ whose domain $\mathbb{C}$ is the direct product of the real numbers with the interval $[0,2\pi)$. The notation $A\{\rho,\mu;\xi,\theta\}$ will be used interchangeably with $A_\mu\rho(\xi,\theta)$ to denote the transformed function which is the attenuated Radon transform of ρ with respect to the attenuation distribution μ evaluated at ξ and θ. Recall that the Radon transform is a special case of the attenuated Radon transform, that is, $\mu = 0$ everywhere. Therefore A_0 will be used to denote the Radon transform.

If A_μ maps the Hilbert space X of concentration functions ρ into the Hilbert space Y of projection functions p, then the range and the null space of the linear operator A_μ is denoted as $\mathcal{R}(A_\mu) \subseteq Y$ and $\mathcal{N}(A_\mu) \subseteq X$, respectively. The adjoint operator of A_μ, denoted by A_μ^*, maps the Hilbert space Y into X and is defined such that $\langle \rho, A_\mu^* p \rangle = [A_\mu \rho, p]$ for all $\rho \in X$ and $p \in Y$, where $\langle\ ,\ \rangle$ and $[\ ,\ ]$ are the inner products in the Hilbert space X and Y, respectively. If $A_\mu : X \to Y$ is a bounded linear operator, then $\mathcal{N}(A_\mu)$ and $\mathcal{N}(A_\mu^*)$ are closed subspaces of X and Y, respectively; and $X = \mathcal{N}(A_\mu) + \mathcal{N}(A_\mu)^\perp$ and $Y = \mathcal{N}(A_\mu^*) + \mathcal{N}(A_\mu^*)^\perp$, where the notation $S^\perp$ denotes the orthogonal component of S.

One particular Hilbert space we will consider is $L^2(\mathbb{R}^2, W)$, which represents the space of real valued functions that are square integrable with respect to the weight function W. It will be shown in section 4 that with properly chosen weight functions the attenuated Radon transform maps this Hilbert space into the Hilbert space $L^2(\mathbb{C}, w)$ of the projection functions p defined on the set $\mathbb{C}$ which are square integrable with respect to the weight function w. The inner product for $L^2(\mathbb{R}^2, W)$ is

$$(2.4) \qquad \langle \rho, \rho' \rangle_{\mathbb{R}^2, W} = \iint_{\mathbb{R}^2} \rho(x,y)\ \rho'(x,y)\ W(x,y)\ dxdy \quad ,$$

and the inner product for $L^2(\mathbb{C}, w)$ is

$$(2.5) \qquad [p, g]_{\mathbb{C}, w} = \iint_{\mathbb{C}} p(\xi,\theta)\ g(\xi,\theta)\ w(\xi,\theta)\ d\xi d\theta \quad .$$

The adjoint transform of the attenuated Radon transform $A_\mu : L^2(\mathbb{R}^2,W) \to L^2(\mathbb{C},w)$ is

$$(2.6) \qquad (A_\mu^* g)(x,y) = \frac{1}{W(x,y)} \int_0^{2\pi} g(-x \sin\theta + y \cos\theta,\theta)$$

$$\times \; a(x,y -x \sin\theta + y \cos\theta,\theta)\; w(-x \sin\theta + y \cos\theta,\theta) d\theta \; ,$$

where

$$a(x,y,-x \sin\theta + y \cos\theta,\theta) =$$

$$(2.7) \qquad \exp\left[-\int_{x\cos\theta + y\sin\theta}^{\infty} \mu\Big(x \sin^2\theta - y \cos\theta \sin\theta + \zeta' \cos\theta,\right.$$

$$\left. -x \sin\theta \cos\theta + y \cos^2\theta + \zeta' \sin\theta\Big) d\zeta'\right] \; .$$

By the property of functionals on Hilbert spaces, we know that $A_\mu^* g$ is unique. The adjoint transform A_μ^* is an inverse mapping in the sense that it maps the Hilbert space of projection functions $L^2(\mathbb{C},w)$ into the Hilbert space of concentration functions $L^2(\mathbb{R}^2,W)$.

Another operator which operates on $L^2(\mathbb{C},w)$ is the back-projection operator B_μ defined by

$$(2.8) \qquad (B_\mu g)(x,y) = \int_0^{2\pi} \frac{g(-x \sin\theta + y \cos\theta,\theta)}{a(x,y,-x \sin\theta + y \cos\theta,\theta)} \, d\theta \quad .$$

This operator differs from the adjoint transform ((2.6)) in that the weighting functions W and w do not appear and the attenuation factor is equal to the reciprocal of the attenuation factor given in (2.7). Both the adjoint transform A_μ^* and the back-projection operator B_μ can be considered as "back-projection" operators since they both assign a value for the point (x,y) which corresponds to back-projecting the projection values for all projection rays passing through the same point (x,y) weighted by the appropriate weighting functions and attenuation factors.

3. <u>The single-angle projection operator</u>. The single-angle projection operator $A_{\mu,\theta}$ is defined as $(A_{\mu,\theta}\rho)(\xi) = (A_\mu\rho)(\xi,\theta)$ so that $A_{\mu,\theta}\rho$ is a single projection at the angle θ. In this section we will investigate some of the properties of the single-angle projection operator $A_{\mu,\theta}$ which are extensions of the results developed by Marr [50] for the Radon transform. The goal is to define an operator which is a modification of the attenuated Radon transform so that we can look at some interesting Hilbert spaces in which this operator composed with its adjoint is an "into" mapping. This then gives us a hint as to how to proceed when we look at the continuous angle case.

In the following theorems we will use the attenuation function a given by (2.7) as a weight function for the Hilbert space $L^1(\mathbb{R}^2,a)$. Functions $\rho \in L^1(\mathbb{R}^2,a)$ satisfy

$$\iint_{\mathbb{R}^2} |\rho(x,y)|\ a(x,y,-x\sin\theta + y\cos\theta,\theta)\, dxdy \ < \ \infty \ .$$

The weight function $a(x,y,-x\sin\theta + y\cos\theta,\theta)$ represents the line integral of the attenuation coefficients from the point (x,y) to ∞ in the direction of the vector $\underset{\sim}{\theta}^{\perp} = (\cos\theta,\sin\theta)$. The inner product for the Hilbert space $L^1(\mathbb{R}^2,a)$ is given by

$$<f,g>_{\mathbb{R}^2,a} = \iint_{\mathbb{R}^2} f(x,y)\ g(x,y)\ a(x,y,-x\sin\theta + y\cos\theta,\theta)\, dxdy \ .$$

THEOREM 1. For any θ, $A_{\mu,\theta}$ is a bounded linear map from $L^1(\mathbb{R}^2,a)$ into $L^1(\mathbb{R})$ with $\|A_{\mu,\theta}\| = 1$.

PROOF. Using the definition $(A_{\mu,\theta}\,\rho)(\xi) = (A_\mu\,\rho)(\xi,\theta)$ and the definition of A_μ given by (2.2) we have

$$\begin{aligned}\int_{\mathbb{R}} |(A_{\mu,\theta}\,\rho)(\xi)|d\xi &= \int\left|\int \rho(-\xi\sin\theta + \zeta\cos\theta,\ \xi\cos\theta + \zeta\sin\theta)\right. \\ &\quad \left.\times\ a(\zeta,\xi,\theta)d\zeta\right|d\xi \\ &\leqslant \iint_{\mathbb{R}^2} |\rho(-\xi\sin\theta + \zeta\cos\theta,\ \xi\cos\theta + \zeta\sin\theta) \\ &\quad \times\ a(\zeta,\xi,\theta)|\,d\zeta d\xi \quad .\end{aligned}$$

Using Fubini's theorem, we have for $\rho \in L'(\mathbb{R}^2,a)$:

$$\int_{\mathbb{R}^2} |(A_{\mu,\theta}\rho)(\xi)|d\xi \leqslant \iint_{\mathbb{R}^2} \left|\rho(x,y)\ a(x,y,-x\sin\theta + y\cos\theta,\theta)\right|dxdy < \infty\,. \tag{3.1}$$

Therefore $A_{\mu,\theta}\,\rho \in L^1(\mathbb{R})$. Rewriting (3.1), we can express this as

$$\|A_{\mu,\theta}\,\rho\| \leqslant \|\rho\| \quad .$$

This implies that

$$\|A_{\mu\ \theta}\| = \sup_{\|\rho\| \leqslant 1} \frac{\|A_{\mu,\theta}\,\rho\|}{\|\rho\|} \leqslant 1 \quad .$$

If we let $\rho(x,y) = \delta(x)\ \delta(y)\ [a(x,y,-x\sin\theta + y\cos\theta,\theta)]^{-1}$ we see that $\|A_{\mu,\theta}\| = 1$. Q.E.D.

Next we want to consider the adjoint operator of $A_{\mu,\theta}: L^1(\mathbb{R}^2,a) \to L^1(\mathbb{R})$. The inner product for the Hilbert space $L^1(\mathbb{R})$ is given by $[p,q]_{\mathbb{R}} = \int_{\mathbb{R}} p(\xi)\, q(\xi) d\xi$. Therefore, using this definition and the corresponding definition of inner product for the Hilbert space $L^1(\mathbb{R}^2,a)$, one can show that the adjoint operator $A^*_{\mu,\theta}$ maps the function h defined on $\mathbb{R}$ into the function $A^*_{\mu,\theta}\, h$ given by

$$(A^*_{\mu,\theta}\, h)(x,y) = h(-x \sin\theta + y \cos\theta) \quad . \tag{3.2}$$

The function $A^*_{\mu}\, h$ is a ridge function [47] which is constant along lines that are parallel to $\underset{\sim}{\theta}^{\perp} = (\cos\theta, \sin\theta)$.

DEFINITION. The function $\chi \in L^1(\mathbb{R}^2,a)$ will denote the characteristic function for a subset Ω of R^2 (i.e., $\chi = 1$ for points in the subset Ω and 0 otherwise) and $\hat{\chi}_{\mu,\theta} = A_{\mu,\theta}\, \chi$. The operator M_f will denote the multiplication operator such that $(M_f\, g)(x,y) = f(x,y)\, g(x,y)$.

THEOREM 2. For $\chi \in L^1(\mathbb{R}^2,a)$

$$(A_{\mu,\theta}\, M_\chi\, A^*_{\mu,\theta})h = M_{\hat{\chi}_{\mu,\theta}}\, h \quad . \tag{3.3}$$

PROOF. By the definition of $A^*_{\mu,\theta}$ in (3.2), we have $(A^*_{\mu,\theta}\, h)(x,y) = h(-x \sin\theta + y \cos\theta)$. Applying the operator M_χ to this gives $\chi(x,y) \times h(-x \sin\theta + y \cos\theta)$. Therefore the expression on the left in

(3.3) is given by

$$(A_{\mu,\theta} M_\chi A^*_{\mu,\theta} h)(\xi) = \iint_{\mathbb{R}^2} \chi(x,y)\ h(-x \sin\theta + y \cos\theta)\ a(x,y,\xi,\theta)$$

$$\times\ \delta(\xi + x \sin\theta - y \cos\theta)\ dxdy \quad .$$

Using the transformation of coordinates (2.1) we have

$$(A_{\mu,\theta} M_\chi A^*_{\mu,\theta}\ h)(\xi) = \int_{-\infty}^{\infty} \chi(\zeta,\xi,\theta)\ h(\xi)\ a(\zeta,\xi,\theta)d\zeta$$

$$= h(\xi)\ \hat{\chi}_{\mu,\theta}(\xi) = (M_{\hat{\chi}_{\mu,\theta}}\ h)(\xi) \quad . \qquad \text{Q.E.D.}$$

DEFINITION. The θ-silhouette of Ω is the set $\hat{\Omega}_\theta = \{\langle \underset{\sim}{r},\underset{\sim}{\theta} \rangle\ |\underset{\sim}{r} \in \Omega\}$. The intersection of the line $\xi + x \sin\theta - y \cos\theta = 0$ and the set Ω is $\Omega_{\xi,\theta}$.

THEOREM 3. The operator $A_{\mu,\theta}$ maps $L^1(\Omega,a)$ onto $L^1(\hat{\Omega}_\theta)$ with $\|A_{\mu,\theta}\| = 1$.

PROOF. To show that $A_{\mu,\theta}$ is an into mapping, follow steps similar to those in Theorem 1. To show that it is an onto mapping, take a function $h \in L^1(\hat{\Omega}_\theta)$ and let

$$(3.4) \qquad \rho(x,y) = \chi(x,y) \frac{h(-x \sin\theta + y \cos\theta)}{\hat{\chi}_{\mu,\theta}(-x \sin\theta + y \cos\theta)} \quad .$$

Using (2.2) and (2.3),

$$(A_{\mu,\theta}\,\rho)(\xi) = \int\limits_{\Omega_{\xi,\theta}} \chi(\zeta,\xi,\theta)\,\frac{h(\xi)}{\hat{\chi}_{\mu,\theta}(\xi)}\,a(\zeta,\xi,\theta)d\zeta$$

$$= \hat{\chi}_{\mu,\theta}(\xi)\,\frac{h(\xi)}{\hat{\chi}_{\mu,\theta}(\xi)} = h(\xi) \quad .$$

To show that ρ in (3.4) is in $L^1(\Omega,a)$ we have, using Schwartz's inequality and applying Fubini's theorem,

$$\iint\limits_{\Omega} |\rho(x,y)|\; a(x,y,-x\sin\theta + y\cos\theta,\theta)dxdy$$

$$= \iint\limits_{\Omega} \left|\chi(x,y)\,\frac{h(-x\sin\theta + y\cos\theta)}{\hat{\chi}_{\mu,\theta}(-x\sin\theta + y\cos\theta)}\right| a(x,y,-x\sin\theta$$

$$+ y\cos\theta,\theta)dxdy = \iint\limits_{\Omega} \left|\chi(\zeta,\xi,\theta)\,\frac{h(\xi)}{\hat{\chi}_{\mu,\theta}(\xi)}\right| a(\zeta,\xi,\theta)d\zeta d\xi$$

$$= \int\limits_{\hat{\Omega}_{\theta}} |h(\xi)|d\xi \quad .$$

Since $h \in L^1(\hat{\Omega}_{\theta})$ then $\rho \in L^1(\Omega,a)$. To show that the norm of $A_{\mu,\theta}$ is equal to one follows immediately from steps similar to those given in Theorem 1. Q.E.D.

Next we want to define a new single-angle projection operator for the attenuated Radon transform. It will be shown that this operator has an important application in defining an ART algorithm for reconstructing attenuated projection data.

DEFINITION. For a set $\Omega \subseteq \mathbb{R}^2$ with characteristic function χ, the operators $R_{\mu,\theta}$ and $R^*_{\mu,\theta}$ are defined as follows

$$(3.5) \quad \text{i)} \qquad R_{\mu,\theta} = M_{(\hat{\chi}_{\mu,\theta})^{-1}} A_{\mu,\theta} \quad ,$$

$$(3.6) \quad \text{ii)} \qquad R^*_{\mu,\theta} = M_{\chi} A^*_{\mu,\theta} \quad ,$$

where $A^*_{\mu,\theta}$ is defined by (3.2).

THEOREM 4. For any θ and any bounded open set $\Omega \subseteq \mathbb{R}^2$ the following are true:

(i) $R_{\mu,\theta}$ maps $L^2(\Omega,a)$ onto $L^2(\hat{\Omega}_\theta, \hat{\chi}_{\mu,\theta})$.

(ii) The composite operator $R_{\mu,\theta} R^*_{\mu,\theta}$ is an identity on $L^2(\hat{\Omega}_\theta, \hat{\chi}_{\mu,\theta})$.

(iii) The composite operator $R^*_{\mu,\theta} R_{\mu,\theta}$ is an idempotent operator — i.e., $(R^*_{\mu,\theta} R_{\mu,\theta})^2 = R^*_{\mu,\theta} R_{\mu,\theta}$.

PROOF. (i) Using Schwartz's inequality and the definitions of $A_{\mu,\theta}$ in (2.2) and $R_{\mu,\theta}$ in (3.5), we see from the following sequence of inequalities that $R_{\mu,\theta}$ maps $L^2(\Omega,a)$ into $L^2(\hat{\Omega}_\theta, \hat{\chi}_{\mu,\theta})$:

$$\begin{aligned} |(A_{\mu,\theta}\, \rho)(\xi)| &= \left| \int_{\Omega_{\xi,\theta}} \rho(\zeta,\xi,\theta)\, \chi(\zeta,\xi,\theta)\, a(\zeta,\xi,\theta) d\zeta \right| \\ &\leq \left(\int_{\Omega_{\xi,\theta}} |\rho(\zeta,\xi,\theta)|^2\, a(\zeta,\xi,\theta) d\zeta \right)^{\frac{1}{2}} \left(\int_{\Omega_{\xi,\theta}} \chi(\zeta,\xi,\theta)\, a(\zeta,\xi,\theta) d\zeta \right)^{\frac{1}{2}} \\ &\leq \left(\int_{\Omega_{\xi,\theta}} |\rho(\zeta,\xi,\theta)|^2\, a(\zeta,\xi,\theta) d\zeta \right)^{\frac{1}{2}} [\hat{\chi}_{\mu,\theta}(\xi)]^{\frac{1}{2}} \quad . \end{aligned}$$

For $\rho \in L^2(\Omega,a)$

$$\int_{\hat{\Omega}_\theta} \left| \frac{(A_{\mu,\theta}\rho)(\xi)}{\hat{\chi}_{\mu,\theta}(\xi)} \right|^2 \chi_{\mu,\theta}(\xi)d\xi \leqslant \left(\iint_\Omega |\rho(\zeta,\xi,\theta)|^2 \, a(\zeta,\xi,\theta)d\zeta d\xi \right) < \infty$$

Therefore, $R_{\mu,\theta}\,\rho = M_{(\hat{\chi}_{\mu,\theta})^{-1}} \, A_{\mu,\theta}\,\rho \in L^2(\hat{\Omega}_\theta,\hat{\chi}_{\mu,\theta})$.

To show that $R_{\mu,\theta}$ is an onto mapping, take a function $h \in L^2(\hat{\Omega}_\theta, \hat{\chi}_{\mu,\theta})$ and let

$$\rho(x,y) = \chi(x,y) \, h(-x \sin\theta + y \cos\theta) \quad .$$

Then using (2.2), (2.3), and (3.5),

$$(R_{\mu,\theta}\rho)(\xi) = \frac{1}{\hat{\chi}_{\mu,\theta}(\xi)} \int_{\Omega_{\xi,\theta}} \chi(\zeta,\xi,\theta) \, h(\xi) \, a(\zeta,\xi,\theta)d\zeta$$

$$= h(\xi) \quad .$$

To show that $\rho \in L^2(\Omega,a)$ we have, using Schwartz's inequality and Fubini's theorem,

$$\left(\iint_\Omega |\rho(x,y)|^2 \, a(x,y,-x \sin\theta + y \cos\theta,\theta)dxdy \right)^{\frac{1}{2}}$$

$$= \left(\iint_\Omega |\chi(x,y) \, h(-x \sin\theta + y \cos\theta)|^2 \, a(x,y,-x \sin\theta +$$

$$+ \, y \cos\theta,\theta)dxdy \right)^{\frac{1}{2}} = \left(\iint_\Omega \chi(\zeta,\xi,\theta) \, |h(\xi)|^2 \, a(\zeta,\xi,\theta)d\zeta d\xi \right)^{\frac{1}{2}}$$

$$= \left(\int_{\hat{\Omega}_\theta} |h(\xi)|^2 \, \hat{\chi}_{\mu,\theta}(\xi)d\xi \right)^{\frac{1}{2}} < \infty \quad .$$

(ii) The proof that $R_{\mu,\theta} R^*_{\mu,\theta}$ is an identity on $L^2(\hat{\Omega}_\theta, \hat{\chi}_{\mu,\theta})$ follows immediately from Theorem 2 and the fact that $\hat{\chi}_{\mu,\theta}(\xi) \neq 0$ for $\xi \in \hat{\Omega}_\theta$

(iii) Using the result in (ii) we have

$$\begin{aligned}(R^*_{\mu,\theta} R_{\mu,\theta})^2 &= R^*_{\mu,\theta} R_{\mu,\theta} R^*_{\mu,\theta} R_{\mu,\theta} \\ &= R^*_{\mu,\theta} 1 R_{\mu,\theta} \\ &= R^*_{\mu,\theta} R_{\mu,\theta} \quad . \qquad \text{Q.E.D.}\end{aligned}$$

COROLLARY 4.1. For any function $\rho \in L^2(\Omega,a)$ the operator $P_{\mu,\theta}$ operating on ρ' defined as

$$P_{\mu,\theta}\, \rho' = \rho' + R^*_{\mu,\theta} R_{\mu,\theta}(\rho - \rho') \quad ,$$

is a projection operator mapping $L^2(\Omega,a)$ onto the subspace $\rho + \mathcal{N}(R_{\mu,\theta})$.

PROOF. The operator $P_{\mu,\theta}$ is an idempotent operator, which can be shown as follows

$$\begin{aligned}P_{\mu,\theta}(P_{\mu,\theta}\, \rho') &= P_{\mu,\theta}\, \rho' + R^*_{\mu,\theta} R_{\mu,\theta}(\rho - P_{\mu,\theta}\rho') \\ &= \rho' + R^*_{\mu,\theta} R_{\mu,\theta}(\rho-\rho') + R^*_{\mu,\theta} R_{\mu,\theta}[\rho-\rho' - R^*_{\mu,\theta}R_{\mu,\theta}(\rho-\rho')] \ .\end{aligned}$$

By Theorem 4 (iii) we know that $(R^*_{\mu,\theta}R_{\mu,\theta})^2 = (R^*_{\mu,\theta}R_{\mu,\theta})$, and therefore

$$\begin{aligned}P_{\mu,\theta}(P_{\mu,\theta}\, \rho') &= \rho' + R^*_{\mu,\theta}R_{\mu,\theta}(\rho-\rho') + R^*_{\mu,\theta}R_{\mu,\theta}(\rho-\rho') - R^*_{\mu,\theta}R_{\mu,\theta}(\rho-\rho') \\ &= \rho' + R^*_{\mu,\theta}R_{\mu,\theta}(\rho-\rho') \ .\end{aligned}$$

Further, one can show that $P_{\mu,\theta}$ is Hermitian and the subspace $\rho + \mathcal{N}(R_{\mu,\theta})$ is equal to $\{\rho' | P_{\mu,\theta}\,\rho' = \rho'\}$. Using [30, Theorem 3, p.44], we know that $P_{\mu,\theta}$ is a projection operator mapping $L^2(\Omega,a)$ onto the subspace $\rho + \mathcal{N}(R_{\mu,\theta})$. Q.E.D.

This result has important application in developing an algorithm for determining a solution to a finite set of projections $R_{\mu,\theta_1}\rho$, $R_{\mu,\theta_2}\,\rho, \ldots, R_{\mu,\theta_N}\,\rho$. The algorithm is due to Kaczmarz [31],[41] and in computed tomography is more commonly called ART [27]. The concentration functions which have the same projections as the solution ρ are those in the subspace $\mathcal{M} = \left(\rho + \bigcap_{i=1}^{N} \mathcal{N}(R_{\mu,\theta_i})\right)$. If $P_{\mu,N}$ is the projection operation given by

$$P_{\mu,N} = \prod_{i=1}^{N} P_{\mu,\theta_i} \quad ,$$

then for an initial guess ρ_o the theorem due to Kaczmarz shows that $P^K_{\mu,N}\,\rho_o$ converges to the projection of ρ_o on $\mathcal{M}$ [31]. If ρ_o is chosen to be zero, then $P^K_{\mu,N}\rho_o$ converges to the unique function $\hat{\rho}$ of smallest norm that satisfies $R_{\mu,\theta_i}\,\rho = R_{\mu,\theta_i}\,\hat{\rho}$ for $i = 1,\ldots,N$.

4. The Continuous-Angle Projection Operator. In this section we will investigate the attenuated Radon transform given in (2.2) for continuous angle. First we will look at some shift properties, then our investigation will lead to a discussion of the generalized inverse and some of the spectral considerations for this transform.

The following theorem gives the result for attenuated projections when both the concentration distribution and attenuation distribution are shifted relative to a fixed coordinate system. The proof follows immediately using (2.2) and is proven in detail in [28].

THEOREM 5. The attenuated Radon transform of $\rho(x+a,y+b)$ with respect to the attenuation coefficient distribution $\mu(x+a,y+b)$ is

$$(4.1) \qquad A\{\rho(x+a,y+b),\ \mu(x+a,y+b);\xi,\theta\} = A\{\rho(x,y),\ \mu(x,y);\xi',\theta\},$$

where $\xi' = \xi - a\sin\theta + b\cos\theta$.

This result will become useful in section 5 when we digitize the reconstruction domain and consider transforms of characteristic functions over square pixels. If we know the transform at the origin we can invoke the shift property given in Theorem 5 and evaluate the attenuated Radon transform of characteristic functions over any region in $\mathbb{R}^2$.

The result in Theorem 5 requires that the distribution of attenuation coefficients μ translate in the same manner as the emitter concentration ρ. If we compare this with the situation where μ is held fixed, then we get a different result:

THEOREM 6. The attenuated Radon transform A_μ of $\rho(x+a,y+b)$ is given by

$$(4.2) \qquad A\{\rho(x+a,y+b),\ \mu(x,y);\xi,\theta\} = A\{\rho(x,y),\ \mu(x-a,y-b);\xi',\theta\},$$

where $\xi' = \xi - a\sin\theta + b\cos\theta$.

This shows how the projection data will change when the concentration is shifted within a fixed attenuator. This has practical application for *in vivo* dynamic studies.

The results given in Theorems 1, 2, 3 and 4 used the attenuation function $a(x,y,-x \sin\theta + y \cos\theta,\theta)$ as a weight function for the L^1 and L^2 spaces. Since $a(x,y,-x \sin\theta + y \cos\theta,\theta)$ is a function of θ, we define a new weight function $\tilde{a}(x,y)$, which is independent of θ, in order to generalize the results for a single projection angle to continuous angle:

$$(4.3) \qquad \tilde{a}(x,y) = \sup_{\theta} \left\{ a(x,y,-x \sin\theta + y \cos\theta,\theta) \right\} .$$

The function $\tilde{a}(x,y)$ represents the minimum attenuation that photons emitted at (x,y) can possibly experience. Using $\tilde{a}$ as a weight function, one can show that A_μ maps $L^1(\mathbb{R}^2,\tilde{a})$ into $L^1(\mathbb{C})$. The adjoint operator for this mapping is given in (2.6), where $W = \tilde{a}$ and $w = 1$:

$$(4.4) \qquad (A_\mu^* g)(x,y) = \frac{1}{\tilde{a}(x,y)} \int_0^{2\pi} g(-x \sin\theta + y \cos\theta,\theta) \times a(x,y,-x\sin\theta + y\cos\theta,\theta)\, d\theta \quad .$$

In the following discussion we will investigate mappings on $L^2(\mathbb{R}^2, \tilde{a} W)$, where W is an arbitrary nonzero positive weight function. This differs from section 3 where we restricted the concentration functions to be defined on a bounded open set $\Omega \subset \mathbb{R}^2$. This approach is very much akin to applying the Radon transform A_0 to the function space $L^2(\mathbb{R}^2,e^{x^2+y^2})$. Later we will see that for this case the operator $A_0 A_0^*$ is Hermitian and has eigenfunctions which involve the Legendre polynomials.

DEFINITION. For a positive weight function W defined on $\mathbb{R}^2$, the operators R_μ and R_μ^* are defined as follows:

$$(4.5)\quad \text{i)}\qquad R_\mu = M_{(A_\mu W^{-1})^{-1}} A_\mu \quad ,$$

$$(4.6)\quad \text{ii)}\qquad R_\mu^* = M_{(W)^{-1}} A_\mu^* \quad .$$

where A_μ^* is given in (4.4). The notation W^{-1} does not mean the inverse mapping but the reciprocal function $1/W$.

THEOREM 7. For a positive nonzero weight function W defined on $\mathbb{R}^2$ and $1/W \in L^2(\mathbb{R}^2)$, the following are true:

i) R_μ maps $L^2(\mathbb{R}^2, \tilde{a}\, W)$ into $L^2(\mathbb{C}, A_\mu(W)^{-1})$,

ii) R_μ^* maps $L^2(\mathbb{C}, A_\mu(W)^{-1})$ into $L^2(\mathbb{R}^2, \tilde{a}\, W)$.

PROOF. (i) Using Schwartz's inequality and the definition of A_μ in (2.2), we see that

$$\begin{aligned} |(A_\mu\rho)(\xi,\theta)| &= \left| \int_{-\infty}^{\infty} \rho(\zeta,\xi,\theta)\, a(\zeta,\xi,\theta)\, d\zeta \right| \\ &\leq \left(\int_{-\infty}^{\infty} |\rho(\zeta,\xi,\theta)|^2\, a(\zeta,\xi,\theta)\, W(\zeta,\xi,\theta)\, d\zeta \right)^{\frac{1}{2}} \\ &\quad \times \left(\int_{-\infty}^{\infty} a(\zeta,\xi,\theta)/W(\zeta,\xi,\theta)\, d\zeta \right)^{\frac{1}{2}} \\ &\leq \left(\int_{-\infty}^{\infty} |\rho(\zeta,\xi,\theta)|^2\, a(\zeta,\xi,\theta)\, W(\zeta,\xi,\theta) d\zeta \right)^{\frac{1}{2}} \left\{ [A_\mu(W)^{-1}](\xi,\theta) \right\}^{\frac{1}{2}} \end{aligned}$$

Since $a(\zeta,\xi,\theta) \leq \tilde{a}(\zeta,\xi,\theta)$ where $\tilde{a}$ is given in (4.3),

$$|(A_\mu\rho)(\xi,\theta)| \leqslant \left(\int_{-\infty}^{\infty} |\rho(\zeta,\xi,\theta)|^2\ \tilde{a}(\zeta,\xi,\theta)\ W(\zeta,\xi,\theta)d\zeta\right)^{\frac{1}{2}} \left\{[A_\mu(W)^{-1}](\xi,\theta)\right\}^{\frac{1}{2}} .$$

The condition that W be a nonzero weight function insures that $[A_\mu(W)^{-1}](\xi,\theta)$ is nonzero. If $\rho \in L^2(R^2, \tilde{a}\,W)$ then by Fabini's theorem,

$$\left(\int_{\mathbb{C}} \left|\frac{(A_\mu\rho)(\xi,\theta)}{[A_\mu(W)^{-1}](\xi,\theta)}\right|^2 [A_\mu(W)^{-1}](\xi,\theta)d\xi d\theta\right)^{\frac{1}{2}}$$

$$\leqslant \left(\int_{\mathbb{R}^2} |\rho(x,y)|^2\ \tilde{a}(x,y)\ W(x,y)dxdy\right)^{\frac{1}{2}} < \infty \quad .$$

Therefore $R_\mu\rho = M_{[A_\mu(W)^{-1}]^{-1}}\, A_\mu\rho \ \in\ L^2(\mathbb{C},A_\mu(W)^{-1})$.

(ii) Using Schwartz's inequality and the definition of R^*_μ in (4.6), we have the following sequence of inequalities:

$$(R^*_\mu\ h)(x,y) = \frac{1}{\tilde{a}(x,y)W(x,y)} \int_0^{2\pi} h(-x\sin\theta + y\cos\theta,\theta)\ a(x,y,-x\sin\theta + y\cos\theta,\theta)d\theta$$

$$\leqslant \frac{1}{\tilde{a}(x,y)W(x,y)} \left(\int_0^{2\pi} h^2(-x\sin\theta + y\cos\theta,\theta)\ a(x,y,-x\sin\theta + y\cos\theta,\theta)d\theta\right)^{\frac{1}{2}}$$

$$\times \left(\int_0^{2\pi} a(x,y,-x\sin\theta + y\cos\theta,\theta)d\theta\right)^{\frac{1}{2}}$$

$$|(R^*_\mu\ h)(x,y)|^2\ \tilde{a}(x,y)W(x,y) \leqslant \frac{1}{W(x,y)} \int_0^{2\pi} h^2(-x\sin\theta + y\cos\theta,\theta)$$

$$\times\ a(x,y,-x\sin\theta + y\cos\theta,\theta)d\theta \int_0^{2\pi} \frac{a(x,y,-x\sin\theta + y\cos\theta,\theta)}{\tilde{a}(x,y)}\, d\theta$$

Since $a(x,y,-x\sin\theta + y\cos\theta,\theta) \leqslant \tilde{a}(x,y)$, we know that the second integral is less than or equal to 2π. Integrating over $\mathbb{R}^2$ and using Fubini's theorem, we have for $h \in L^2(\mathbb{C},A_\mu(W)^{-1})$,

$$\int_{\mathbb{R}^2} |(R_\mu^* h)(x,y)|^2\, \tilde{a}(x,y)W(x,y)dxdy \leqslant \int_{\mathbb{R}^2} \frac{2\pi}{W(x,y)} \int_0^{2\pi} h^2(-x\sin\theta + y\cos\theta,\theta)$$

$$\times\ a(x,y,-x\sin\theta + y\cos\theta,\theta)d\theta\ dx\ dy$$

$$\leqslant \int_{\mathbb{R}^2} \frac{2\pi}{W(x,y)} \int_{\mathbb{C}} h^2(\xi,\theta)\ a(x,y,\xi,\theta)$$

$$\times\ \delta(\xi + x\sin\theta - y\cos\theta)d\xi d\theta\ dxdy$$

$$\leqslant 2\pi \int_{\mathbb{C}} h^2(\xi,\theta)\ [A_\mu(W)^{-1}](\xi,\theta)d\xi d\theta\ < \infty .$$

Therefore, $R_\mu^* h \in L^2(\mathbb{R}^2,\tilde{a}W)$. Q.E.D.

An approach to solving the reconstruction problem in single-photon ECT involves evaluating the generalized inverse of the attenuated Radon transform. We will first define the generalized inverse in the context of emission tomography. Then we will show that if the composition of R_μ and R_μ^* has an L^2 kernel [20] then the attenuated Radon transform and its generalized inverse can be decomposed and represented as a sum of eigenfunctions. The kernel for the composite operators $R_\mu R_\mu^*$ and $R_\mu^* R_\mu$ will be evaluated; however, we cannot give an explicit expression for their eigenfunctions.

4.1. The generalized inverse. The generalized inverse is an operator which is applicable to both finite and infinite dimensional Hilbert spaces. Before the widespread use of the generalized inverse in matrix theory [5],[6], it was developed to determine the solution to integral and differential equations [60]. We will develop the concepts of generalized inverse in a manner similar to that given by Kammerer and Nashed [42].

Reconstructing attenuated data for a known attenuation distribution requires solving the linear operator equation

$$R_\mu(\rho) = p_o \quad , \tag{4.7}$$

where $R_\mu : X \to Y$ is the operator given by (4.5), ρ is the distribution of isotope concentration, and p_o is the projection. The concentration $\hat{\rho} \in X$ is called the best approximate solution of (4.7) if $\inf\{\| R_\mu(\rho) - p_o\| \,|\, \rho \in X\} = \| R_\mu(\hat{\rho}) - p_o\|$. This is equivalent to minimizing $\|p - p_o\|$ over all $p \in \mathcal{R}(R_\mu)$. The minimum $\hat{p}$, characterized by the condition $p_o - \hat{p}$, is orthogonal to the space $\mathcal{R}(R_\mu)$ (i.e., $p_o - \hat{p} \in \mathcal{R}(R_\mu)^\perp$), which is equivalent to $p_o - \hat{p} \in \mathcal{N}(R_\mu^*)$. This implies that $R_\mu^* R_\mu(\rho) = R_\mu^*(p_o)$. Therefore, $\hat{\rho} \in X$ is a best approximate solution of (4.7) if and only if it is a solution of the equation

$$R_\mu^* R_\mu(\rho) = R_\mu^*(p_o) \quad . \tag{4.8}$$

The linear manifold $\mathcal{R}(R_\mu)$ may not be closed in Y. Therefore, the orthogonal projection of p_0 onto $\overline{\mathcal{R}(R_\mu)}$ may not be in $\mathcal{R}(R_\mu)$ and (4.7) and (4.8) do not have a solution. However, if we only consider those projection functions which are in $\mathcal{R}(R_\mu) + \mathcal{R}(R_\mu)^\perp$ (if $\mathcal{R}(R_\mu)$ is closed then $\mathcal{R}(R_\mu) + \mathcal{R}(R_\mu)^\perp = Y$), the solution to (4.7) is determined by evaluating the generalized inverse R_μ^G of the operator R_μ. R_μ^G is the mapping whose domain is given by $\mathcal{D}(R_\mu^G) = \mathcal{R}(R_\mu) + \mathcal{R}(R_\mu)^\perp$, such that for $p \in \mathcal{D}(R_\mu^G)$,

$$(4.9) \qquad R_\mu^G p = \rho_0 \in S = \{\hat\rho \in X \,|\, \inf \| R_\mu(\rho) - p \| = \| R_\mu(\hat\rho) - p \| \;,\; \rho \in X\}$$

and $\|\rho_0\| < \|\hat\rho\|$ for all $\hat\rho \in S$, $\hat\rho \neq \rho_0$. Therefore for each $p \in \mathcal{R}(R_\mu) + \mathcal{R}(R_\mu)^\perp = \mathcal{D}(R_\mu^G)$, $R_\mu^G(p)$ is a unique solution. The set S of all best approximate solutions of (4.7) for a fixed $p_0 \in \mathcal{D}(R_\mu^G)$ is given by

$$(4.10) \qquad R_\mu^G\, p_0 + \mathcal{N}(R_\mu^* R_\mu) = R_\mu^G\, p_0 + \mathcal{N}(R_\mu) \quad .$$

It can be seen from (4.10) that the null space of the operator R_μ is a measure of non-uniqueness.

Next we will derive a formula for the generalized inverse when the operator R_μ is compact. If R_μ is compact, then $\mathcal{R}(R_\mu)$ is closed and $\mathcal{R}(R_\mu) + \mathcal{R}(R_\mu)^\perp = Y$.

4.2. The singular value decomposition. From (4.8) we see that the generalized inverse of R_μ is closely related to the generalized inverse of the self-adjoint operator $R_\mu^* R_\mu$. In fact,

$$\rho_o = R^G p_o = (R_\mu^* R_\mu)^G R_\mu^*(p_o) \quad . \tag{4.11}$$

In the discussion to follow we will show that the knowledge of the eigenfunctions of $R_\mu^* R_\mu$ and $R_\mu R_\mu^*$ lead to a singular value decomposition of R_μ and R_μ^G.

If $\mathcal{R}(R_\mu)$ is closed, then by the closed-range theorem [74], $\mathcal{R}(R_\mu^*)$ is also closed and $\mathcal{R}(R_\mu^*) = \mathcal{N}(R_\mu)^\perp = \mathcal{R}(R_\mu^* R_\mu)$. In this case the operator $R_\mu^* R_\mu$ restricted to the space $\mathcal{R}(R_\mu^*) = \mathcal{N}(R_\mu)^\perp$ is a one-to-one and onto mapping of $\mathcal{N}(R_\mu)^\perp$ onto itself. The operator $R_\mu^* R_\mu : \rho \to \beta$ is given by a Fredholm integral equation of the first kind:

$$\beta(x',y') = \iint \rho(x,y)\, K(x',y'|x,y)\, dxdy \quad , \tag{4.12}$$

where K is the kernal of the transformation. For the Radon transform $A_o : L^2(\mathbb{R}^2) \to L^2(\mathbb{C})$ this kernel is the well-known function

$$(4.13) \qquad K(x',y'|x,y) = \frac{2}{\| \underset{\sim}{r} - \underset{\sim}{r}' \|} ,$$

where $\underset{\sim}{r} = (x,y)$ and $\underset{\sim}{r}' = (x',y')$ and for which the result in (4.12) is a convolution.

The following theorem gives the kernel K for the operator $R_\mu^* R_\mu$. The space of projection functions $L^2(\mathbb{C},w)$ has the weight function

$$w(\xi,\theta) = (A_\mu \, 1/W)(\xi,\theta) ,$$

where W is a nonzero positive function on $\mathbb{R}^2$ and $1/W \in L^2(\mathbb{R}^2)$.

THEOREM 8. The composition of the adjoint operator R_μ^* defined by (4.6) and R_μ defined by (4.5) maps $\rho \in L^2(\mathbb{R}^2, \tilde{a}W)$ into $\beta \in L^2(\mathbb{R}^2, \tilde{a}W)$ $(R_\mu^* R_\mu : \rho \to \beta)$, where β is given by (4.12) with the kernel K given by

$$(4.14) \qquad K(x',y'|x,y) = \frac{1}{W(x',y')\tilde{a}(x',y')} \cdot \frac{1}{\| \underset{\sim}{r} - \underset{\sim}{r}' \|}$$

$$\times \left[\exp\left\{ - \int_d^\infty \mu(b+\zeta' e, c+\zeta' f)\, d\zeta' - \int_{d'}^\infty \mu(b+\zeta' e, c+\zeta' f)\, d\zeta' \right\} \frac{1}{w(\xi,\theta_1)} \right.$$

$$\left. + \exp\left\{ - \int_{-d}^\infty \mu(b-\zeta' e, c-\zeta' f)\, d\zeta' - \int_{-d'}^\infty \mu(b-\zeta' e, c-\zeta' f)\, d\zeta' \right\} \frac{1}{w(-\xi,\theta_2)} \right]$$

where

$$(4.15) \qquad \sin\theta_1 = \frac{y-y'}{\| \underset{\sim}{r} - \underset{\sim}{r}' \|} , \qquad \cos\theta_1 = \frac{x-x'}{\| \underset{\sim}{r} - \underset{\sim}{r}' \|} ,$$

$$\sin\theta_2 = \frac{-(y-y')}{\|\underset{\sim}{r}-\underset{\sim}{r}'\|}, \qquad \cos\theta_2 = \frac{-(x-x')}{\|\underset{\sim}{r}-\underset{\sim}{r}'\|}, \tag{4.16}$$

$$\xi = \frac{-x(y-y')}{\|\underset{\sim}{r}-\underset{\sim}{r}'\|} + \frac{y(x-x')}{\|\underset{\sim}{r}-\underset{\sim}{r}'\|}, \tag{4.17}$$

$$d = \frac{x(x-x') + y(y-y')}{\|\underset{\sim}{r}-\underset{\sim}{r}'\|} = \frac{\langle \underset{\sim}{r}, (\underset{\sim}{r}-\underset{\sim}{r}')\rangle}{\|\underset{\sim}{r}-\underset{\sim}{r}'\|}, \tag{4.18}$$

$$d' = \frac{x'(x-x') + y'(y-y')}{\|\underset{\sim}{r}-\underset{\sim}{r}'\|} = \frac{\langle \underset{\sim}{r}', (\underset{\sim}{r}-\underset{\sim}{r}')\rangle}{\|\underset{\sim}{r}-\underset{\sim}{r}'\|}, \tag{4.19}$$

$$b = \frac{(y-y')\ (yx'-xy')}{\|\underset{\sim}{r}-\underset{\sim}{r}'\|^2}, \tag{4.20}$$

$$c = \frac{(x-x')(xy'-yx')}{\|\underset{\sim}{r}-\underset{\sim}{r}'\|^2}, \tag{4.21}$$

$$e = \frac{(x-x')}{\|\underset{\sim}{r}-\underset{\sim}{r}'\|}, \tag{4.22}$$

$$f = \frac{(y-y')}{\|\underset{\sim}{r}-\underset{\sim}{r}'\|}. \tag{4.23}$$

PROOF. See the proof of Theorem 3.3 in [28].

The angles θ_1 and θ_2 in Fig. 3 are the two projection angles at which the points $\underset{\sim}{r}$ and $\underset{\sim}{r}'$ will project along the same line. The arguments for the exponentials in (4.14) represent the integrals of the attenuation coefficient between the point $\underset{\sim}{r}$ and the detector and the point $\underset{\sim}{r}'$ and the detector for the projection angles θ_1 and θ_2, respectively. Therefore, the function K is proportional to the inverse of the distance between the two points $\underset{\sim}{r}$ and $\underset{\sim}{r}'$ times the weighted sum of attenuation factors which represent the attenuation between the respective points $\underset{\sim}{r}$ and $\underset{\sim}{r}'$ and the detectors as viewed from angles 180° apart.

It follows from the next theorem that the kernel function for the composite of the attenuated Radon transform and the back-projection operator given in (2.8) allows us to write (4.12) as a convolution only if the attenuation distribution is constant.

THEOREM 9. For the back-projection operator B_μ defined by (2.8), the operator $B_\mu A_\mu : \rho \to \beta$ maps ρ into β where β is given by (4.12) with the kernel given by

$$(4.24) \qquad K(x',y'|x,y) = \frac{2}{\|\underset{\sim}{r} - \underset{\sim}{r}'\|} \cosh\left\{\int_{d}^{d'} \mu(b+\zeta' e,\ c+\zeta' f)\,d\zeta'\right\} ,$$

where d, d', b, c, e, and f are given by (4.18)-(4.23).
For the Radon transform A_0, it has been shown by [2],[12],[29] that representing (4.11) as a convolution leads to an efficient Fourier filter algorithm which is able to deconvolve the back-projected image β to obtain the reconstructed image $\hat{\rho}$. However, for the attenuated Radon

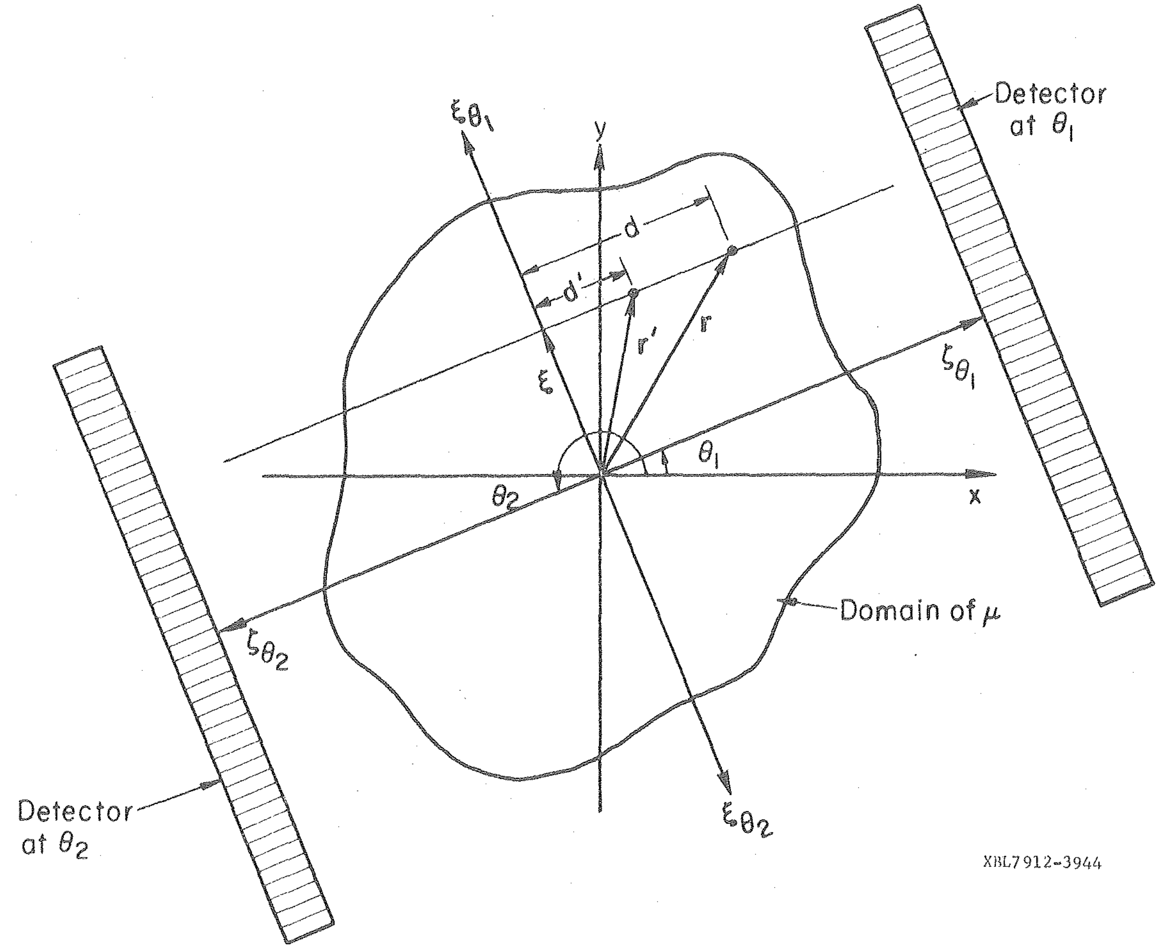

XBL7912-3944

Fig. 3. The integrals in the first exponential of (4.14) are the line integrals of the attenuation distribution μ along the line from the points $\underset{\sim}{r}$ and $\underset{\sim}{r}'$, respectively, in the direction of the detector at θ_1. The integrals in the second exponential of (4.14) are the line integrals of μ along the line from the points $\underset{\sim}{r}$ and $\underset{\sim}{r}'$, respectively, in the direction of the detector at θ_2.

transform, (4.12) is a convolution only if μ is constant. Even then if $\mu > 0$, an algorithm cannot be devised since the back-projected image β does not have a finite Fourier transform.

In the previous discussion we evaluated in Theorem 8 the kernel for the operator $R_\mu^* R_\mu$. Next we want to do likewise for $R_\mu R_\mu^*$. If $\mathcal{R}(R_\mu)$ is closed, we know by the closed-range theorem that $\mathcal{R}(R_\mu) = \mathcal{N}(R_\mu^*)^\perp = \mathcal{R}(R_\mu R_\mu^*)$. Since the solution to (4.7) is equivalent to minimizing $\| p - p_0 \|$ over all $p \in \mathcal{R}(R_\mu)$, then when $\mathcal{R}(R_\mu)$ is closed the solution to (4.7) is equivalent to minimizing $\| R_\mu R_\mu^* p - p_0 \|$ over all $p \in \mathcal{R}(R_\mu R_\mu^*)$. This gives a different formulation of the reconstruction problem, namely, the solution to the linear operator equation

$$R_\mu R_\mu^* p = p_0 \quad , \tag{4.25}$$

where the reconstructed isotope concentration function $\hat{\rho}$ is given by $\hat{\rho} = R_\mu^* \hat{p}$, such that $\hat{p}$ is the best approximate solution to (4.25).

The operator $R_\mu R_\mu^*$ restricted to the space $\mathcal{R}(R_\mu)$ is a one-to-one and onto mapping of $\mathcal{N}(R_\mu^*)^\perp$ onto itself. The mapping $R_\mu R_\mu^* : p \to g$ is given by

$$g(\xi,\theta) = \iint p(\xi',\theta') \, I(\xi,\theta|\xi',\theta') \, d\xi' d\theta' \quad , \tag{4.26}$$

where I is the kernel of the transformation. For the Radon transform $A_0 : L^2(\mathbb{R}^2) \to L^2(\mathbb{C})$, this kernel is

$$I(\xi,\theta|\xi',\theta') = \frac{1}{|\sin(\theta - \theta')|} \quad . \tag{4.27}$$

THEOREM 10. The composition of the operator R_μ defined by (4.5) and R_μ^* defined by (4.6) maps $p \in L^2(\mathbb{C},w)$ into $g \in L^2(\mathbb{C},w)(R_\mu R_\mu^*: p \to g)$ where g is given by (4.26) with the kernel I given by

$$I(\xi,\theta|\xi',\theta') = \frac{\tilde{I}(\xi,\theta|\xi',\theta')}{W(x^*,y^*)\, \tilde{a}(x^*,y^*)\, w(\xi,\theta)} \tag{4.28}$$

where

$$\tilde{I}(\xi,\theta|\xi',\theta') = \frac{1}{|\sin(\theta-\theta')|} \exp\left[-\int_{\zeta_0}^{\infty} \mu(-\xi \sin\theta + \zeta \cos\theta, \xi \cos\theta + \zeta \sin\theta)d\zeta - \int_{\zeta_0'}^{\infty} \mu(-\xi' \sin\theta' + \zeta' \cos\theta', \xi' \cos\theta' + \zeta' \sin\theta')d\zeta'\right] \tag{4.29}$$

and

$$\zeta_0 = \xi \cot(\theta' - \theta) - \xi' \csc(\theta' - \theta) \quad , \tag{4.30}$$

$$\zeta_0' = \xi \csc(\theta' - \theta) - \xi' \cot(\theta' - \theta) \quad , \tag{4.31}$$

$$x^* = \frac{\xi' \cos\theta - \xi \cos\theta'}{\sin(\theta - \theta')} \quad , \tag{4.32}$$

$$y^* = \frac{\xi' \sin\theta - \xi \sin\theta'}{\sin(\theta - \theta')} \quad . \tag{4.33}$$

PROOF. See the proof of Theorem 3.5 in [28].

The coordinates (ζ_0,ξ) and (ζ_0',ξ') are the intersection shown in Fig. 4 of the lines $\xi + x\sin\theta - y\cos\theta = 0$ and $\xi' + x\sin\theta' - y\cos\theta' = 0$ in the $\zeta\xi$- and $\zeta'\xi'$-coordinate system, respectively. The line integrals in (4.29) represent integrals of the attenuation distribution μ along the two lines from the point of intersection.

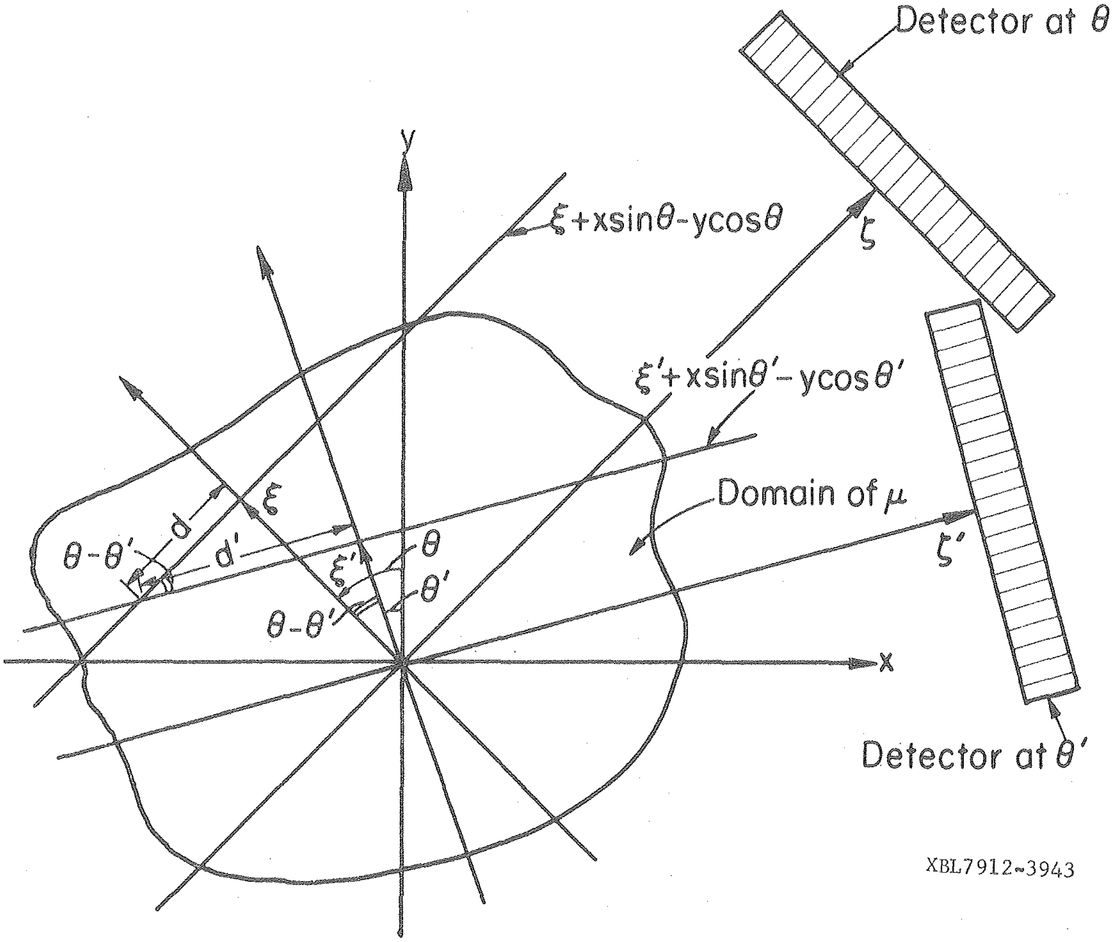

Fig. 4. The first integral in the exponential argument of (4.29) is the line integral of the attenuation distribution μ along the line $\xi + x\sin\theta - y\cos\theta = 0$ from the point of intersection with the line $\xi' + x\sin\theta' - y\cos\theta' = 0$. The second integral is the integral of μ along the line $\xi' + x\sin\theta' - y\cos\theta' = 0$ from the same point of intersection. The distances d and d' satisfy $d = \xi\cot(\theta-\theta') - \xi'\csc(\theta-\theta')$ and $d' = \xi\csc(\theta-\theta') - \xi'\cot(\theta-\theta')$, and the coordinates ζ_0 and ζ_0' satisfy $\zeta_0 = -d$ and $\zeta_0' = -d'$, respectively.

If we examine the kernel given for the Radon transform $A_o : L^2(\mathbb{R}^2) \to L^2(\mathbb{C})$ in (4.13), we see that it is not square integrable (i.e., $\iint\limits_{\mathbb{R}^2} 2/\|\underset{\sim}{r}-\underset{\sim}{r}'\|^2 \, d\underset{\sim}{r} d\underset{\sim}{r}' \not< \infty$). However, if we restrict the space of functions which we will consider by using weight functions $W(x,y)$ and $w(x,y) \neq 1$ for the Hilbert spaces $L^2(\mathbb{R}^2,W)$ and $L^2(\mathbb{C},w)$, we can apply Hilbert-Schmidt theory [55],[65],[73] to determine a singular value decomposition of $R_\mu^* R_\mu$ and $R_\mu R_\mu^*$. We consider only those kernels for these Hermitian operators which are L^2 in the sense that

$$\iint\limits_{\mathbb{R}^2\mathbb{R}^2} \left| K(\underset{\sim}{r}|\underset{\sim}{r}') \right|^2 W(\underset{\sim}{r}) W(\underset{\sim}{r}') \, d\underset{\sim}{r} \, d\underset{\sim}{r}' < \infty \quad ,$$

and

$$\iint\limits_{\mathbb{C}\,\mathbb{C}} \left| I(\underset{\sim}{\omega}|\underset{\sim}{\omega}') \right|^2 w(\underset{\sim}{\omega}) w(\underset{\sim}{\omega}') \, d\underset{\sim}{\omega} \, d\underset{\sim}{\omega} < \infty \quad .$$

The kernel K is Hermitian if $K^*(\underset{\sim}{r}|\underset{\sim}{r}') = K(\underset{\sim}{r}'|\underset{\sim}{r})$ where the adjoint kernel is defined such that $\langle K\rho,\rho' \rangle_{\mathbb{R}^2,W} = \langle \rho, K^*\rho' \rangle_{\mathbb{R}^2,W}$. (Here the notation of $K\rho$ means the same as $R_\mu^* R_\mu$ operating on ρ.) For the Radon transform $A_o : L^2(\mathbb{R}^2,W) \to L^2(\mathbb{C},w)$ with the weight functions $W(x,y) = e^{x^2+y^2}$ and $w(\xi,\theta) = e^{\xi^2}$ [21],[49],[52], the Hermitian L^2 kernel for $A_o^* A_o$ is

$$K(x',y'|x,y) = \frac{2}{\|\underset{\sim}{r} - \underset{\sim}{r}'\|} \exp\left\{ \frac{-\langle \underset{\sim}{r}', \underset{\sim}{r}' - \underset{\sim}{r} \rangle^2}{\|\underset{\sim}{r}' - \underset{\sim}{r}\|^2} \right\} \tag{4.34}$$

and for $A_o A_o^*$ is

$$I(\xi,\theta|\xi',\theta') = \frac{1}{|\sin(\theta-\theta')|} \exp\left\{ \frac{-[\xi' - \xi\cos(\theta-\theta')]^2}{\sin^2(\theta-\theta')} \right\} . \tag{4.35}$$

Other weight functions for the Radon transform have been investigated by Marr [51] and Davison and Grünbaum [17].

If the kernels given by Theorems 8 and 10 for the Hermitian operators $R_\mu^* R_\mu$ and $R_\mu R_\mu^*$ are L^2 kernels, then both have the same set of eigenvalues λ_i. We will denote $\phi_i(x,y)$ to be the eigenfunctions of the operator $R_\mu^* R_\mu$ corresponding to the eigenvalue λ_i and denote $\psi_i(\xi,\theta)$ to be the eigenfunction of the operator $R_\mu R_\mu^*$ corresponding to the same eigenvalue λ_i. The system $(\phi_i,\phi_i;\lambda_i)$ is called a singular system for the kernel K corresponding to $R_\mu^* R_\mu$, and $(\psi_i,\psi_i;\lambda_i)$ is a singular system for the kernel I corresponding to $R_\mu R_\mu^*$ [65]. The eigenfunctions ϕ_i are orthogonal relative to the weight function $W(x,y)$ (i.e., $\iint \phi_i(x,y)\phi_j(x,y)\, W(x,y)dxdy = \delta_{ij}$) and the eigenfunctions ψ_i are orthogonal relative to the weight function $w(\xi,\theta)$. The kernel K corresponding to the operator $R_\mu^* R_\mu$ is a linear combination of $\phi_i(x',y')\phi_i(x,y)$,

$$K(x',y'|x,y) = \sum_{i=1}^{\infty} \lambda_i\, \phi_i(x',y')\, \phi_i(x,y)\, W(x,y) \tag{4.36}$$

[65], and the operator $R_\mu^* R_\mu$ operating on the function $\rho(x,y)$ is

$$(R_\mu^* R_\mu\, \rho)(x',y') = \sum_{i=1}^{\infty} \lambda_i \iint_{\mathbb{R}^2} \rho(x,y)\, \phi_i(x,y)\, W(x,y)dxdy\, \phi_i(x',y'). \tag{4.37}$$

Likewise the kernel I corresponding to the operator $R_\mu R_\mu^*$ is

$$I(\xi,\theta|\xi',\theta') = \sum_{i=1}^{\infty} \lambda_i \psi_i(\xi,\theta)\, \psi_i(\xi',\theta')\, w(\xi',\theta')\ , \tag{4.38}$$

and the operator $R_\mu R_\mu^*$ operating on the function $p(\xi,\theta)$ is given by

$$(R_\mu R_\mu^*\, p)(\xi,\theta) = \sum_{i=1}^{\infty} \lambda_i \iint_{\mathbb{C}} p(\xi',\theta')\, \psi_i(\xi',\theta')\, w(\xi',\theta')d\xi' d\theta'\, \psi_i(\xi,\theta). \tag{4.39}$$

For the Radon transform $A_o: L^2(\mathbb{R}^2, e^{x^2+y^2}) \to L^2(\mathbb{C}, e^{\xi^2})$, the operator $A_o^* A_o$ has the eigenfunctions

$$(4.40) \quad \phi_{nk}(x,y) = (-1)^k \left[\frac{k!}{\pi(|n| + k)!}\right]^{\frac{1}{2}} \left(x + \mathrm{sgn}(n) iy\right)^{|n|} L_k^{|n|}(x^2+y^2) e^{-x^2-y^2} \quad ,$$

where $L_k^{|n|}$ are the Laguerre polynomials. The eigenfunctions ψ_{nk} for the operator $A_o A_o^*$ are

$$(4.41) \qquad \psi_{nk}(\xi,\theta) = \left[2^{2|n|+4k} k!(|n| + k)!\right]^{-\frac{1}{2}} e^{in\theta} H_{|n|+2k}(\xi) e^{-\xi^2} \quad ,$$

where $H_m(\xi)$ is the Hermite polynomial of degree m.

If the eigenvalues λ_i and eigenfunctions ϕ_i and ψ_i are known, then R_μ can be written as

$$(4.42) \qquad (R_\mu \rho)(\xi,\theta) = \sum_{i=1}^{\infty} \lambda_i^{1/2} \iint \rho(x,y)\, \phi_i(x,y)\, W(x,y) dx dy\, \psi_i(\xi,\theta) \quad ,$$

where $(\phi_i, \psi_i; \lambda_i^{\frac{1}{2}})$ is a singular system for R_μ [65]. From this singular value decomposition of R_μ, we can write the generalized inverse as

$$(4.43) \qquad (R_\mu^G\, p_o)(x,y) = \sum_{i=1}^{\infty} \lambda_i^{-1/2} \iint p_\gamma(\xi,\theta)\, \psi_i(\xi,\theta)\, w(\xi,\theta) d\xi d\theta\, \phi_i(x,y).$$

Explicit expressions for the eigenfunctions ϕ_i and ψ_i have not been expressed for R_μ if $\mu > 0$. However, the structure developed in Theorems 8 and 10 guarantee the existence of eigenfunctions if the weight function W is chosen so that the kernels K in (4.14) and I in (4.28) are L^2.

5. A numerical method for reconstructing attenuated projection data.

The practical implementation of inverting the attenuated Radon transform given in (1.2) requires that the relationship between the unknowns representing the distribution of the concentration of radionuclide and the observed projection values be put in a form tractable for digital processing. In this section we will show how the continuous transform reduces to a discrete linear transform that uses a matrix equation to represent data measured at discrete angular and lateral sampling. A complete description of the discrete transform involves obtaining projection data from a transmission experiment and reconstructing these transmission data. Then the reconstruction of the emission data is determined with iterative algorithms that are capable of solving large systems of linear equations [38].

To represent the concentration function ρ and the attenuation function μ digitally, one must parametrize these continuous distributions by a finite array of numbers. The parameters are coefficients of an expansion of basis functions for the continuous distribution. There are many collections of basis functions that can be used; however, the choice depends not only on the errors incurred by the numerical approximation of taking only a finite number of terms in the series expansion, but also on the amplification of statistical noise and the efficiency of calculating the continuous distribution.

We will consider an orthonormal basis which is a set of characteristic functions defined over rectangular pixels. Suppose that the region Ω as shown in Fig. 5 is divided into disjoint rectangular regions called

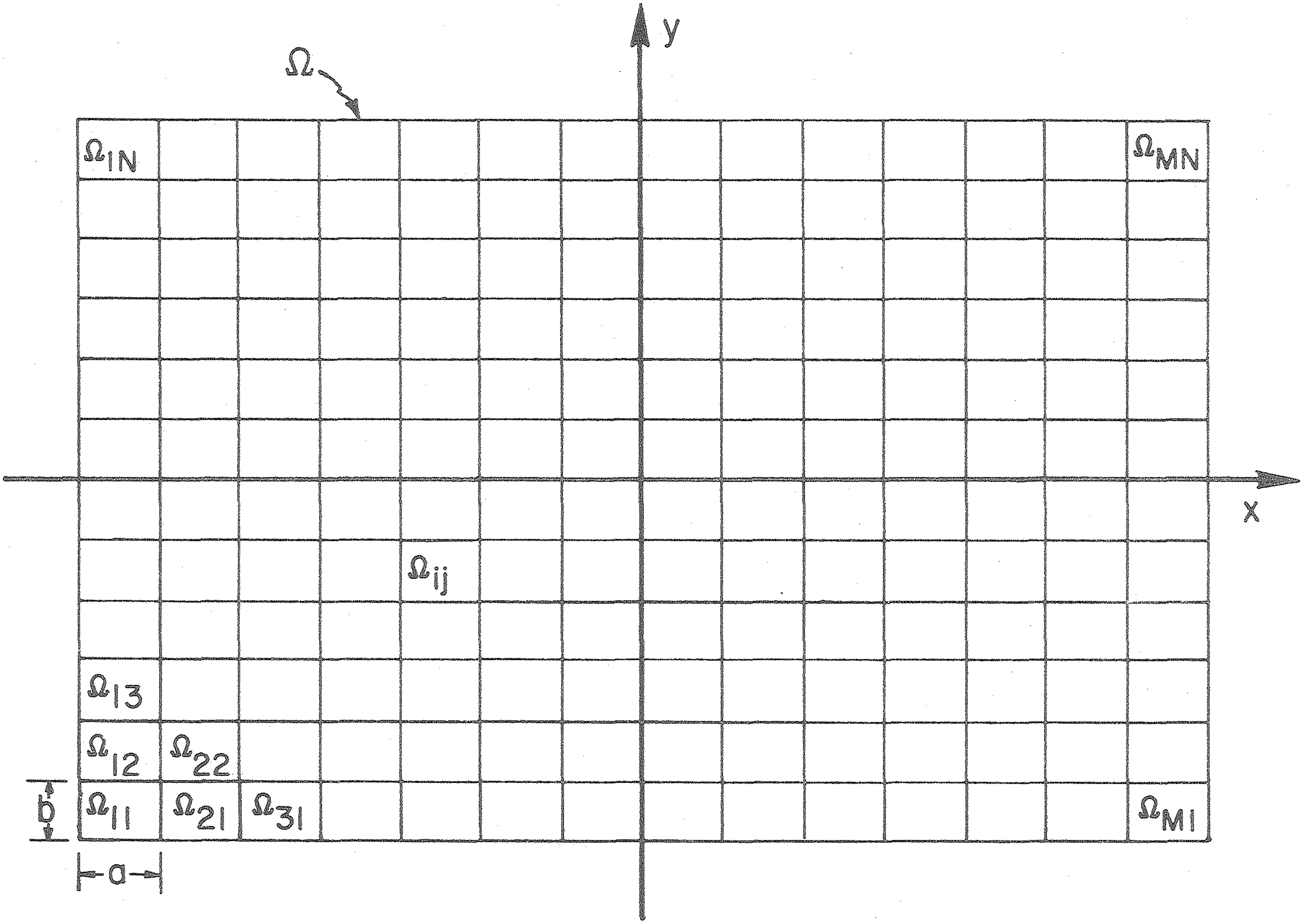

XBL793-3298

Fig. 5. The rectangular region Ω is divided up into disjoint rectangular pixels Ω_{ij} with width a and height b.

pixels for $i = 1, \ldots, M$ and $j = 1, \ldots, N$:

$$\Omega_{ij} = \left\{(x,y) \,\middle|\, \frac{a(2i - M-2)}{2} \leqslant x < \frac{a(2i-M)}{2} \,,\, \frac{b(2j - N-2)}{2} \leqslant y < \frac{b(2j-N)}{2} \right\} ,$$

where a is the width and b is the height of the rectangular pixel Ω_{ij}. Later we will show reconstruction results for square pixels ($a=b$) but for the present we will keep the discussion more general. Over these rectangular regions we define the orthonormal basis as

$$(5.1) \qquad \chi_{ij}(x,y) = \begin{cases} \left(\frac{1}{ab}\right)^{\frac{1}{2}} & \text{if } (x,y) \in \Omega_{ij} \\ 0 & \text{otherwise} \end{cases} .$$

Using these basis functions, we can expand the function ρ as

$$(5.2) \qquad \rho(x,y) = \sum_{i=1}^{M} \sum_{j=1}^{N} \rho_{ij}\, \chi_{ij}(x,y) ,$$

where

$$(5.3) \qquad \rho_{ij} = \left(\frac{1}{ab}\right)^{\frac{1}{2}} \int_{\frac{a(2i-M-2)}{2}}^{\frac{a(2i-M)}{2}} \int_{\frac{b(2j-N-2)}{2}}^{\frac{b(2j-N)}{2}} \rho(x,y)\,dx\,dy .$$

The coefficients ρ_{ij} are the average value of the concentration over the rectangular region Ω_{ij}.

The basis $\{\chi_{ij}\}$ given by (5.1) is referred to by Rosenfeld and Kak [61] as standard sampling and is chosen primarily for its computational efficiency. The disadvantage of choosing these basis functions is that the approximate function ρ can have sharp boundaries [33]. Thus the number of pixels chosen must be large enough to be a good approximation for even a smoothly varying function. A generalization of standard sampling is the finite element approach [67], which uses basis functions that are piecewise linear polynomials in two variables whose supports are polygons that possibly overlap. Other possible basis functions include Fourier and Bessel functions.

The evaluation of the attenuated Radon transform of the basis functions χ_{ij} is simplified if we consider the attenuated Radon transform of the characteristic function of a rectangle with sides a and b positioned at the center of rotation. Then the corresponding transforms of χ_{ij} are obtained using the shift property given in Theorem 5. This gives

$$A\{\chi_{ij}(x,y),\ \mu_{ij}\,\chi_{ij}(x,y);\ \xi,\theta\} =$$

$$(5.4)\quad \begin{cases} 0 & \text{if } \frac{a}{2}|\sin\theta| + \frac{b}{2}|\cos\theta| < \xi + [a(2i-M-1)/2]\sin\theta - [b(2j-N-1)/2]\cos\theta \\ \frac{1}{\mu_{ij}}\left\{1 - \exp\left[-\mu_{ij}\left(\frac{a/2\ |\sin\theta| + b/2\ |\cos\theta| - \xi}{|\cos\theta|\ |\sin\theta|}\right)\right]\right\} & \text{if } \left|\frac{a}{2}|\sin\theta| - \frac{b}{2}|\cos\theta|\right| \le \xi + [a(2i-M-1)/2]\sin\theta - [b(2j-N-1)/2]\cos\theta < -\frac{a}{2}|\sin\theta| + \frac{b}{2}|\cos\theta| \\ \frac{1}{\mu_{ij}}\left\{1 - \exp\left[-\mu_{ij}\frac{a}{|\cos\theta|}\right]\right\} & \text{if } \frac{a}{2}|\sin\theta| - \frac{b}{2}|\cos\theta| \le \xi + [a(2i-M-1)/2]\sin\theta - [b(2j-N-1)/2]\cos\theta < -\frac{a}{2}|\sin\theta| + \frac{b}{2}|\cos\theta| \\ \frac{1}{\mu_{ij}}\left\{1 - \exp\left[-\mu_{ij}\frac{b}{|\sin\theta|}\right]\right\} & \text{if } -\frac{a}{2}|\sin\theta| + \frac{b}{2}|\cos\theta| \le \xi + [a(2i-M-1)/2]\sin\theta - [b(2j-N-1)/2]\cos\theta < \frac{a}{2}|\sin\theta| - \frac{b}{2}|\cos\theta| \\ \frac{1}{\mu_{ij}}\left\{1 - \exp\left[-\mu_{ij}\left(\frac{a/2\ |\sin\theta| + b/2\ |\cos\theta| + \xi}{|\cos\theta|\ |\sin\theta|}\right)\right]\right\} & \text{if } -\frac{a}{2}|\sin\theta| - \frac{b}{2}|\cos\theta| \le \xi + [a(2i-M-1)/2]\sin\theta - [b(2j-N-1)/2]\cos\theta < \left|\frac{a}{2}|\sin\theta| - \frac{b}{2}|\cos\theta|\right| \\ 0 & \text{if } \xi + [a(2i-M-1)/2]\sin\theta - [b(2j-N-1)/2]\cos\theta < -\frac{a}{2}|\sin\theta| - \frac{b}{2}|\cos\theta| \end{cases}$$

The attenuated Radon transform of the radionuclide distribution given by (5.2) with an attenuation distribution

$$(5.5)\qquad \mu(x,y) = \sum_{m=1}^{M}\sum_{n=1}^{N} \mu_{mn}\,\chi_{mn}(x,y)$$

is

$$(5.6) \qquad p(\xi,\theta) = \sum_{i=1}^{M} \sum_{j=1}^{N} \rho_{ij}\, s_{ij}(\xi,\theta) \quad ,$$

where

(5.7)

$$s_{ij}(\xi,\theta) = A\{\chi_{ij}(x,y),\ \mu_{ij}\chi_{ij}(x,y);\xi,\theta\} \exp\left[- \sum_{\substack{m \\ (m,n)\in E_{ij}}} \sum_{n} \mu_{mn} A_o\{\chi_{mn}(x,y);\xi,\theta\}\right]$$

and

(5.8)

$$E_{ij} = \{(m,n) \,|\, ma\cos\theta + nb\sin\theta > ia\cos\theta + jb\sin\theta,\quad 1 \leqslant m \leqslant M,\quad 1 \leqslant n \leqslant N\} \ .$$

The attenuated Radon transform $A\{\chi_{ij}(x,y),\ \mu_{ij}\chi_{ij}(x,y);\xi,\theta\}$ of the characteristic function χ_{ij} is given in (5.4). (This characteristic function has, over its support Ω_{ij}, a constant attenuation coefficient μ_{ij}.) The function $A_o\{\chi_{mn}(x,y);\xi,\theta\}$ is the Radon transform of the characteristic function χ_{mn}.

If the projections given by (5.6) are sampled for a finite number of angles θ_ℓ, $\ell = 1,\ldots,L$ and a finite number of points ξ_k, $k = 1,\ldots,K$ for each angle, then the reconstruction of the radionuclide distribution is the solution to the following system of equations

$$(5.9) \quad \sum_{i=1}^{M} \sum_{j=1}^{N} \rho_{ij}\, s_{ij}(\xi_k,\theta_\ell) = p(\xi_k,\theta_\ell), \qquad \begin{array}{l} k=1,\ldots,K \ ; \\ \ell=1,\ldots,L \ . \end{array}$$

To simplify notation, (5.9) can be rewritten in matrix form by resorting to a lexicographic or stacked notation which contracts the double indices (i,j) and (k,ℓ) to single indices i' and k' respectively. Thus,

$$A\rho = P \quad , \tag{5.10}$$

where A is a $KL \times MN$ matrix with elements $a_{i'k'} = s_{ij}(\xi_k,\theta_\ell)$ such that $i' = (j-1) \times M + i$ and $k' = (\ell-1) \times K + k$. The vector ρ has elements $\rho_{i'} = \rho_{ij}$, and P is a vector with elements $p_{k'} = p_{km}$.

The estimate $\hat{\rho}$ for the radionuclide distribution minimizes the least-squares function

$$X^2(\rho) = (A\rho - P)^T \Phi^{-1} (A\rho - P) \quad , \tag{5.11}$$

where Φ is a covariance matrix for the data and is a symmetric positive semidefinite matrix. The estimate is given by the following two equivalent forms

$$\hat{\rho} = (\Phi^{-\frac{1}{2}} A)^G \Phi^{-\frac{1}{2}} P \quad , \tag{5.12}$$

$$\hat{\rho} = (A^T \Phi^{-1} A)^G A^T \Phi^{-1} P \quad , \tag{5.13}$$

where G denotes the Moore-Penrose generalized inverse [5],[6]. The least squares solution $\hat{\rho}$ is the best approximate solution to the system of equations

$$\Phi^{-\frac{1}{2}} A\rho = \Phi^{-\frac{1}{2}} P \quad , \tag{5.14}$$

and $\hat{\rho}$ is the best approximate solution of (5.14) if and only if $\hat{\rho}$ is a best approximate solution of

$$A^T \Phi^{-1} A\rho = A^T \Phi^{-1} P \quad . \tag{5.15}$$

In most cases the data collected from any patient study requires the determination of a best solution to an inconsistent system of linear equations. The inconsistency in the data comes from such physical factors as statistical noise in the data, inadequacy of the model, and patient movement.

The dimensions of the matrix A are too large in all practical applications so that at present the solution to the best estimate $\hat{\rho}$ cannot be found by matrix inversion using (5.12) or (5.13). Therefore, we must resort to iterative methods to minimize the χ^2 function in (5.11). There are two principal types of iterative reconstruction procedures: (1) those which adjust the parameters involved in one or a small number of projection constraints at each iterative step – the ART-type methods; and (2) those which adjust all the parameters based on information from all the projection samples at each iteration – the SIRT-type methods.

An ART (for Algebraic Reconstruction Techniques) method was first proposed by Gordon, Bender and Herman [27] and is based on a theorem proven by Kaczmarz [41]. A tutorial on ART was later published by Gordon [26] and a description of other ART methods along with optimization criteria and theorems on the convergence of the algorithms to optimum images was given by Herman and Lent [32]. A method for incorporating errors with the ART-type algorithms was described by Huebel and Lantz [37]. For the finite-dimensional case, the proof of convergence for consistent systems is given in [33],[68]. Convergence rates for this iterative procedure are analyzed by Hamaker and Solmon [31]. In ART, a new solution is given by

$$(5.16) \qquad \rho^{n+1} = \rho^n + q^n \quad ,$$

where

$$(5.17) \qquad q^n = a_j^G \{p_j - \langle a_j, \rho^n \rangle\} = \frac{1}{\|a_j\|^2} a_j^T \{p_j - \langle a_j, \rho^n \rangle\} \quad ,$$

$$(5.18) \qquad j = n \bmod KL + 1 \quad , \qquad n = 0,1,2,\ldots \quad .$$

K is the number of projection bins, L is the number of projection angles, a_j is the j-th column of A, and p_j is the j-th projection sample. The operation in (5.16) is equivalent to operating on ρ^n with the discrete analogue of the operator $P_{\mu,\theta}$ in Corollary 4.1, namely, the operator $P_{\mu,j}$:

$$(5.19) \qquad P_{\mu,j}\rho^n = \rho^n + a_j^G \{p_j - \langle a_j, \rho^n \rangle\}.$$

Note that the operator $P_{\mu,\theta}$ represents a continuum of samples at the projection angle θ, whereas $P_{\mu,j}$ corresponds to one projection bin at the angle θ.

SIRT (for Simultaneous Iterative Reconstruction Techniques) methods were first applied to reconstruction tomography by Goitein [25] and Gilbert [24]. Later, steepest descent methods and conjugate gradient methods originally developed by Hestenes and Stiefel [34] were implemented by Huesman and co-workers [38]. A more recent paper about SIRT-type algorithms is by Lakashminarayanan and Lent [46]. These iterative schemes basically determine a direction q^n and a step length α^n for each iteration such that the new solution is given by

$$(5.20) \qquad \rho^{n+1} = \rho^n + \alpha^n q^n \quad .$$

The step length calculation α^n is determined so that $\chi^2(\rho^{n+1}) = \chi^2(\rho^n + \alpha^n q^n)$ is a minimum. It was shown in [38] that Goitein's method is the same as a steepest descent method in a transformed space. In most cases, convergence of the iterative process is accelerated by performing such a scale change on the parameters. The scale change is given by

$$\rho' = D\rho \quad , \tag{5.21}$$

where D is a diagonal matrix with diagonal elements equal to

$$D_{ii} = \left[(A^T \Phi^{-1} A)_{ii}\right]^{\frac{1}{2}} \quad . \tag{5.22}$$

The iterative stepping is performed on the transformed variables ρ' and the final reconstruction is obtained by the operation

$$\rho = D^{-1} \rho' \quad . \tag{5.23}$$

A mathematical approach to analyzing the rates of convergence for steepest descent and conjugate gradient methods is presented in [42] and [54]. Simulations in [28] show that the rate of convergence is a function of the attenuating medium.

6. Applications. The algorithm illustrated in Fig. 6 can be used in single-photon ECT to reconstruct radionuclide distributions from projection data which have been attenuated by a variable attenuation coefficient. This algorithm uses subroutines from the RECLBL Library [38], a package of computational subroutines that apply to the

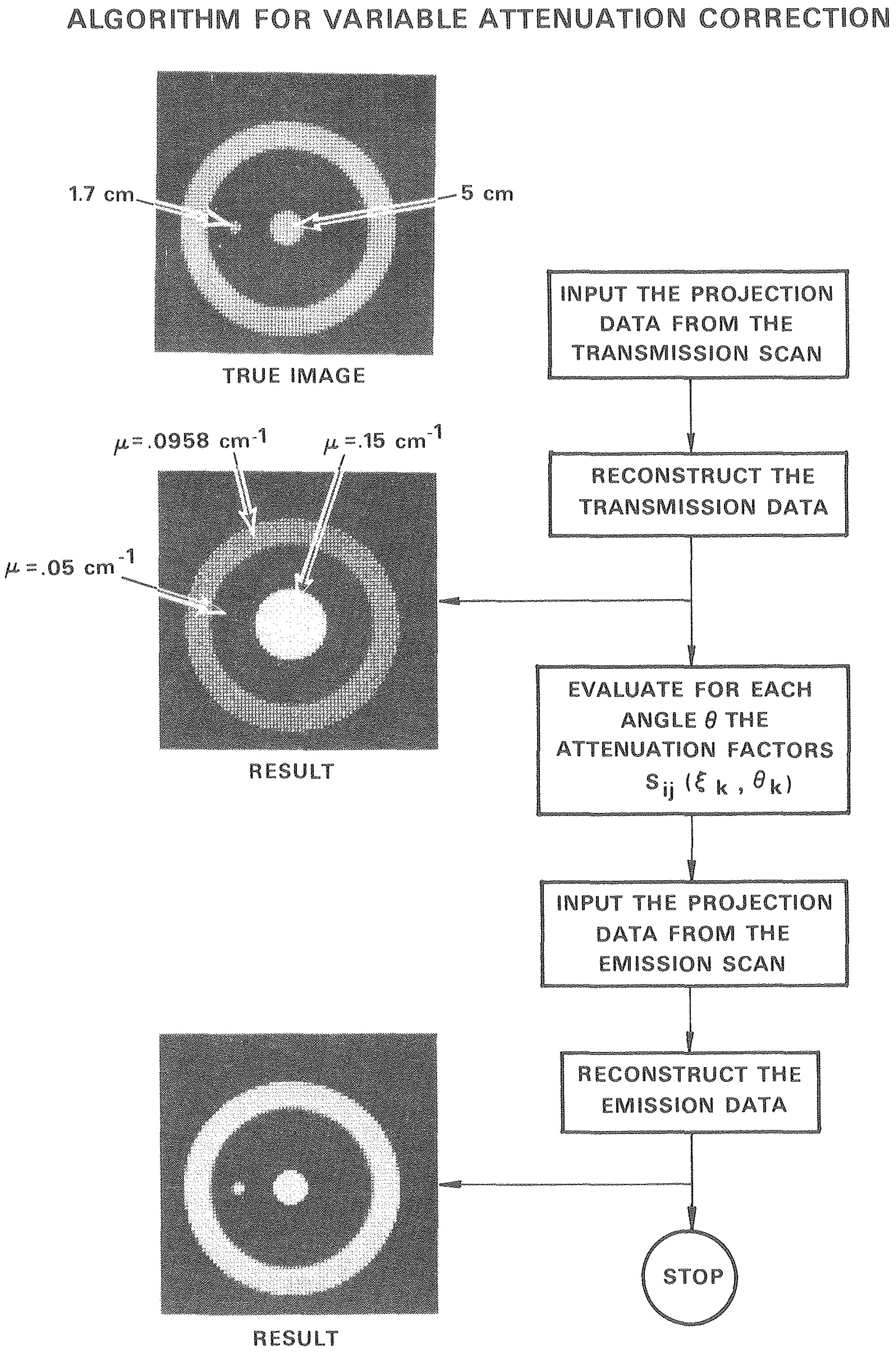

XBB 793-3411

Fig. 6. Algorithm for reconstructing emission data attenuated by a variable attenuation coefficient. Transmission data is reconstructed in order to determine the actual attenuation factors $s_{ij}(\xi_k, \theta_\ell)$ in (5.7). The emission reconstruction uses these factors to compensate for attenuation.

reconstruction of transverse sections from projection data. A transmission reconstruction is first done to accurately determine the attenuation coefficients. Then the factors $s_{ij}(\xi_k,\theta_\ell)$ are evaluated using (5.7). The radionuclide distribution is then reconstructed using an iterative algorithm to fit the emission projection data.

This algorithm requires two reconstructions: one for the transmission data to obtain the attenuation coefficients and one for the emission data to obtain the final reconstruction. Errors in the reconstruction of the attenuation coefficients will increase the errors in the emission reconstruction. These errors in the emission reconstruction are the result of noise propagated from three sources: (1) statistical fluctuations in emission data, (2) statistical fluctuations in the incident transmission beam, and (3) statistical fluctuations in the emerging transmission beam. These sources of errors can be evaluated based on the percent root mean squared (%RMS) uncertainty of the target area of interest. The %RMS uncertainty = $100\,\sigma(\rho)/\bar{\rho}$, where $\sigma(\rho)$ and $\bar{\rho}$ are the sample error and the sample mean, respectively, over a region of a finite number of pixels. Simulations in [28] indicate that the %RMS uncertainty of a distributed source in a 20-cm diameter region with $\mu = 0.15\ \mathrm{cm}^{-1}$ cannot be better than 9.8% even with infinite statistics if the attenuation coefficients are determined using an incident transmission beam of 1000 photons per projection ray (4.2×10^6 total photons).

Single-photon ECT with attenuation compensation has been applied to both human and canine studies using various radionuclides [10]. The ability to image a particular organ depends on the ability of the organ to take up the radionuclide compared to the surrounding tissue, the energy of the emitted photon, and the measured statistics for both emission and transmission. For example, the use of radionuclides for myocardial imaging generally gives a low target-to-nontarget contrast ratio. For high-energy radionuclides such as potassium-43, rubidium-82, rubidium-81 and -82m, and cesium-129, fewer photons are attenuated as compared with Tl-201 and Cs-131; however, the contribution of activity from back muscles and lungs tends to wash out the image on projection [15]. The anterior myocardium is well visualized with lower energy radionuclides such as cesium-131 and thallium-201; but photons from the posterior myocardial wall are greatly attenuated and quantitation of septal and posterior wall defects is seriously limited. The fundamental problem is not so much the specificity of uptake of radionuclide in the organ vs. uptake in the contiguous tissues, but the physical properties of the radionuclide that one can correlate with attenuation coefficients, which in turn dictate the required statistics to insure a desired precision.

Results from a study showing abnormal accumulation of isotope in two tumors in a 50-year-old woman are shown in Fig. 7. This study was done one hour after injection of 15 mCi of ^{99m}Tc-pertechnetate (140 keV). Normal brain tissue is either relatively or completely impermeable to the passage of most radionuclides from the blood. In contrast, brain tumors are much more permeable than normal brain, and this results in a significantly higher relative concentration of radioactivity in the tumor. For the study shown in Fig. 7, the projection data were collected in 10° increments over 360° which gave approximately 240,000 counts per slice. The attenuation coefficient was assumed to be constant.

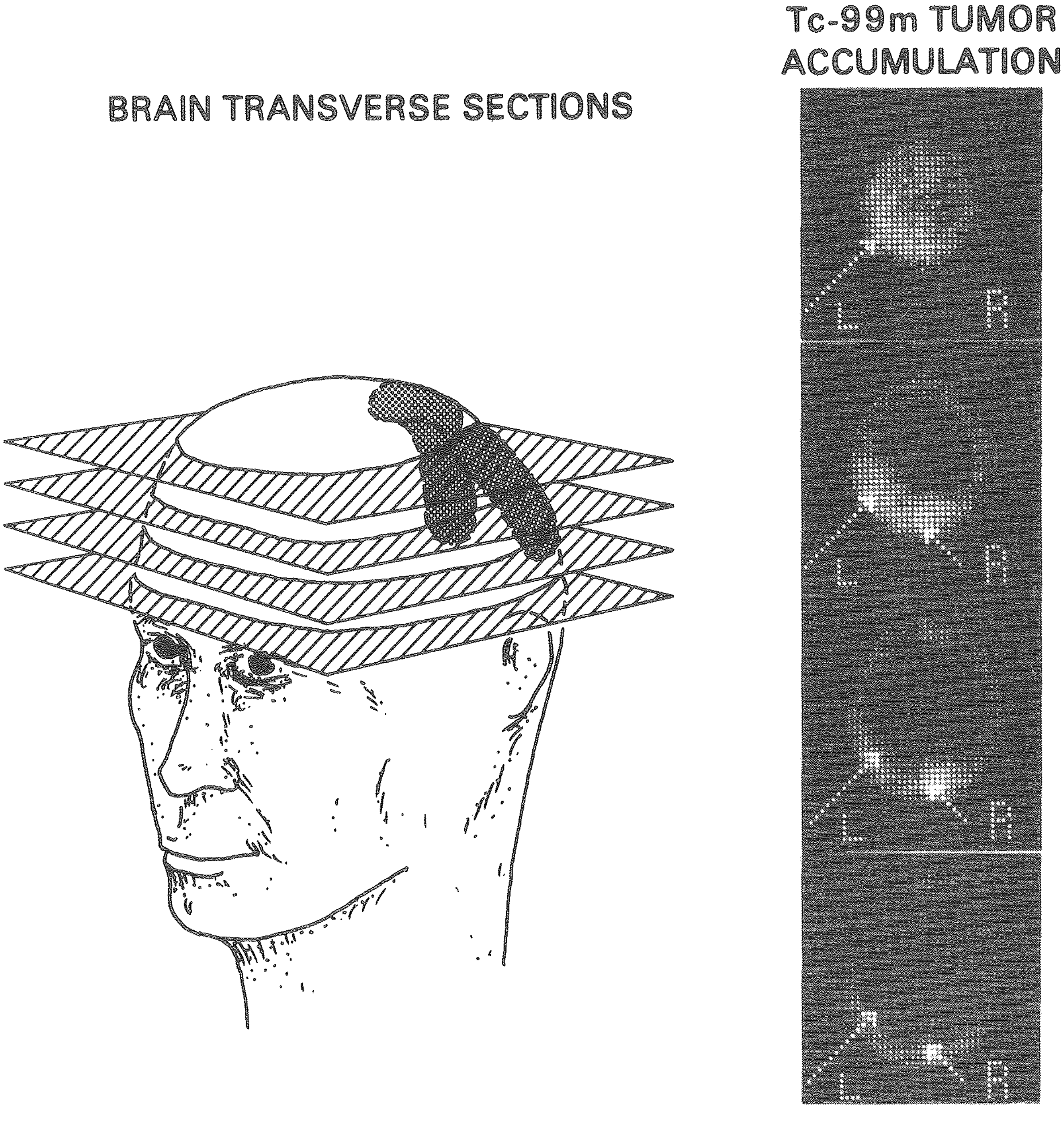

XBB 7711-7514

Fig. 7. Transverse sections showing abnormal accumulation in the head of a 50-year-old patient using ^{99m}Tc-pertechnetate and 36 views. The measured number of emission events for each section are (from bottom to top) 220,582, 251,213, 265,286, and 222,584, respectively.

Simulations done in [28] indicate that for perfect transmission statistics the %RMS uncertainty is between 91.5% and 41.5% for attenuation coefficient $\mu = 0.15\ \text{cm}^{-1}$ and emission counts of 2.5×10^5. This means that tumors with a contrast of 2 to 1 can be seen, but their boundaries are hard to delineate.

Potassium and potassium analogs such as cesium have a high affinity to the heart because of the high muscular and nerve activity. Transverse section images of ^{129}Cs in the human myocardium are shown in Fig. 8 for a patient who had had four myocardial infarctions. The study was done by taking views at 20° increments. A transverse section reconstruction of attenuation coefficients was performed first to correct for attenuation in the emission reconstruction. Section 4 shows a paucity of uptake in the posterior wall and septum consistent with electrocardiographic findings. The left myocardial wall, septum, and right ventricular myocardium are recognizable. The dome of the liver is seen in sections 2 and 3, as would be expected, since the liver accumulates cesium and potassium analogs with about the same avidity as the heart. In order to obtain the correct attenuation coefficients for Cs-129 (375 keV-48%), the results of a transmission study using Tc-99m (140 keV) were extrapolated using the tables in [40] for attenuation coefficient versus energy for tissue, so that the attenuation coefficients corresponded to the 375 keV photons emitted from Cs-129. This means that in tissue the attenuation coefficient is approximately $0.11\ \text{cm}^{-1}$. The transmission study in Fig. 8 has a %RMS uncertainty of at least 15% for an incident number of photons of almost 4000 per projection bin. The %RMS uncertainty in the emission images is approximately 50%.

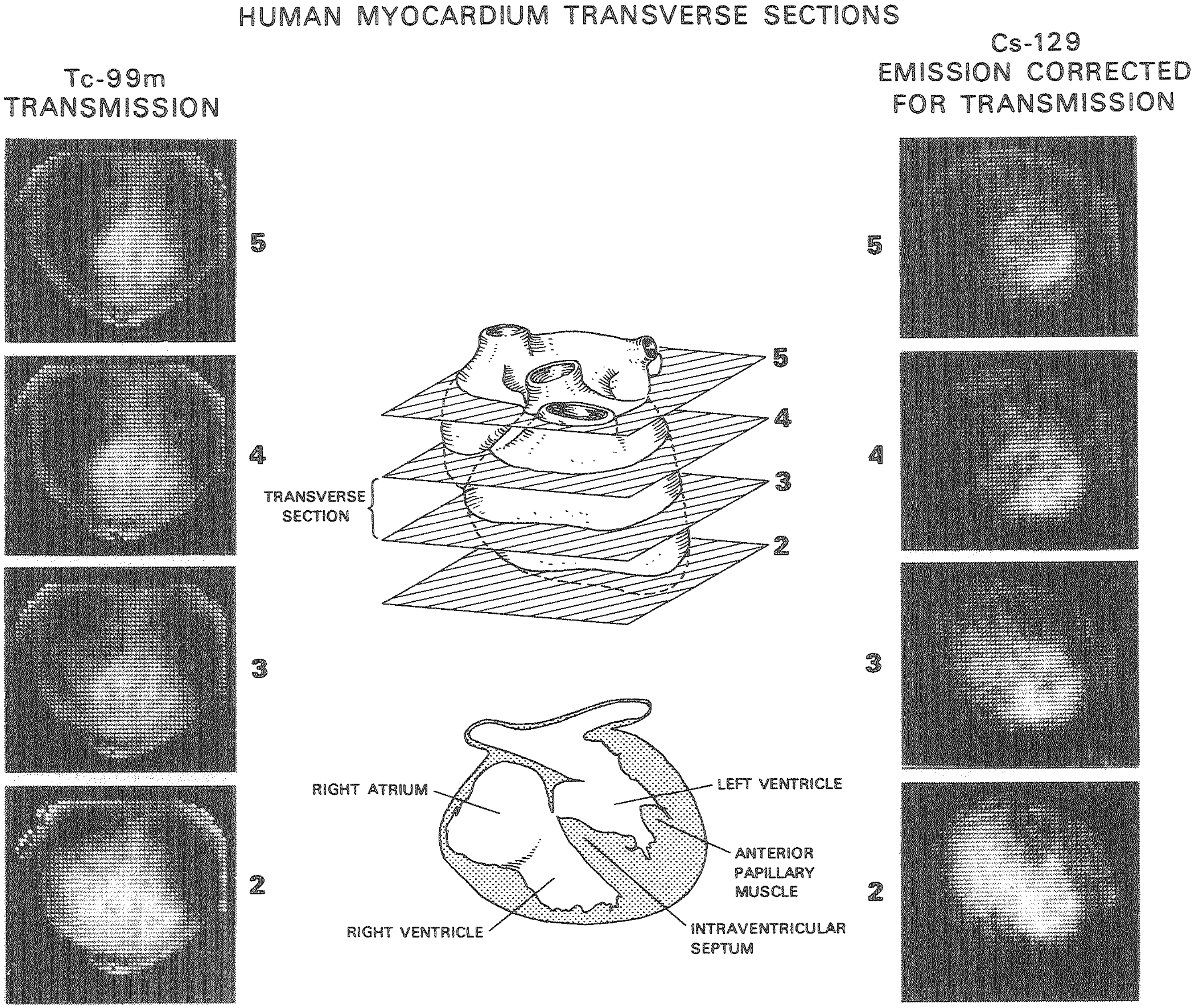

XBB 749-6039

Fig. 8. Transmission and emission transverse sections of the thorax in a 60-year-old patient with four myocardial infarctions. Septal activity normal, but anterolaterial activity low. The measured number of emission events is: plane 2 – 247,903, plane 3 – 233,989, plane 4 – 220,230, plane 5 – 205,529. The incident number of photons per projection bin for the transmission study is: plane 2 – 3,558, plane 3 – 3,801, plane 4 – 3,942, and plane 5 – 3,822.

When injected intravenously, selenomethionine is rapidly removed from the blood and incorporated in protein synthesis. The isotope will eventually reappear in plasma proteins. Selenomethionine concentration in muscle is much lower than in the thyroid, parathyroid, or blood because of the slow turnover rate of muscle protein. A study shown in Fig. 9 was done on a dog to see how well ^{75}Se-selenomethionine (136 keV-57%, 265 keV-60%) is taken up in the heart. On the left are two transverse sections demonstrating the position of the heart in the chest with sufficient resolution to show the esophagus. The accumulation of ^{75}Se in the myocardium is shown on the right. The %RMS uncertainty is at most 90%.

The accumulation of ^{99m}Tc-sulfur colloid in the liver and spleen is shown in the transverse sections of Fig. 10. The Kupffer cells of the liver remove foreign substances from the blood and hence will accumulate the labeled sulfur granules of 1 μm in diameter (see also Fig. 1 and discussion in section 1). The better the liver is functioning, the more ^{99m}Tc attached to sulfur colloid will be available for imaging; that is, the functioning liver becomes labeled. The time required to reach a steady state accumulation is 3 to 5 minutes, and the time during which the distribution of concentration remains constant is 30 minutes or longer. The %RMS uncertainty is at most 41% for the images shown in Fig. 10.

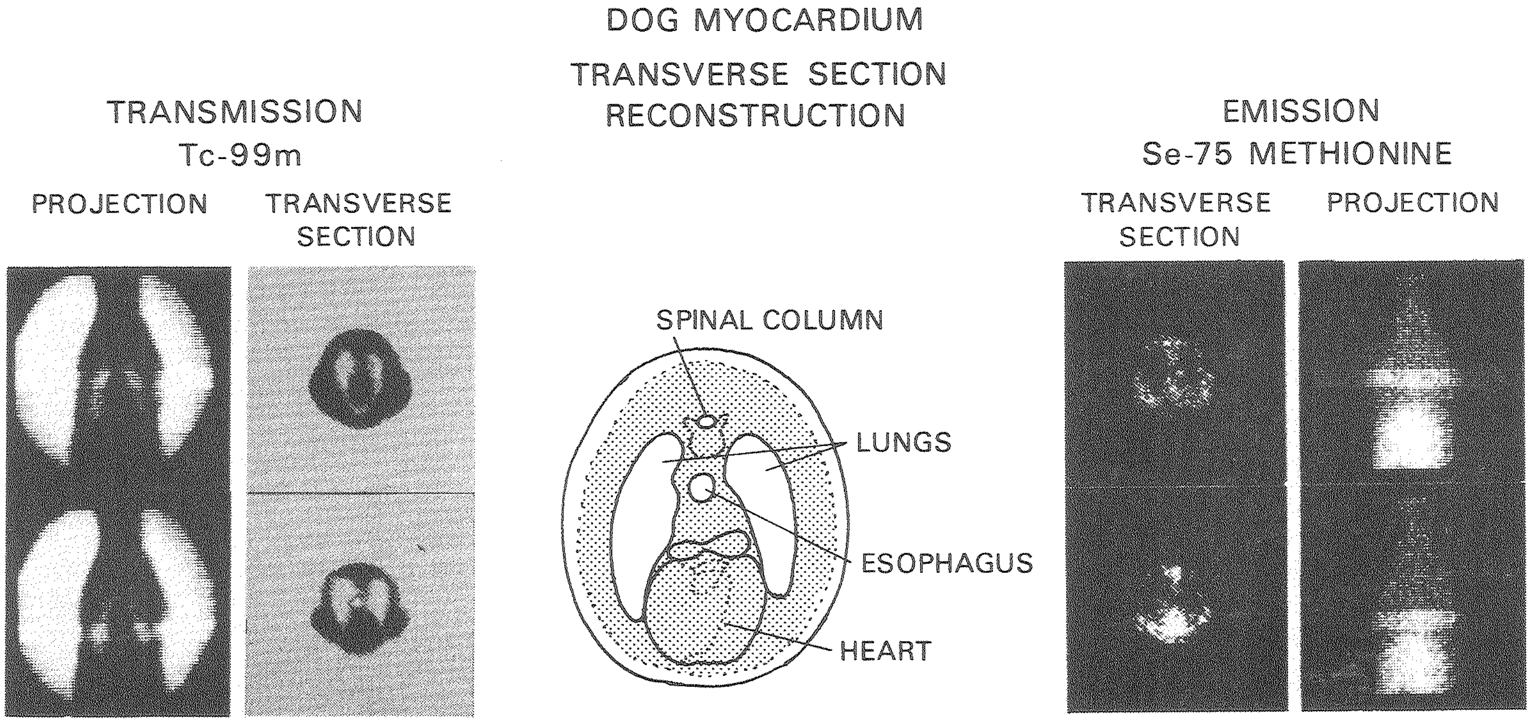

XBB 740-8045

Fig. 9. At the right, accumulation of ^{75}Se-selenomethionine is seen in the dog myocardium after intravenous injection of 750 μCi. These cross-sectional images were reconstructed from 36 projections over 360° with a total of 128,103 events for the bottom image and 113,092 for the top image. The transmission study shown on the left was performed using an 8-mCi point source of ^{99m}Tc, three meters from the subject. This gave an incident number of photons per projection bin for each of the 18 projections over 180° of 4,449 for the bottom cross section and 4,730 for the top cross section. The light bands across the projection images indicate the level for the transverse sections.

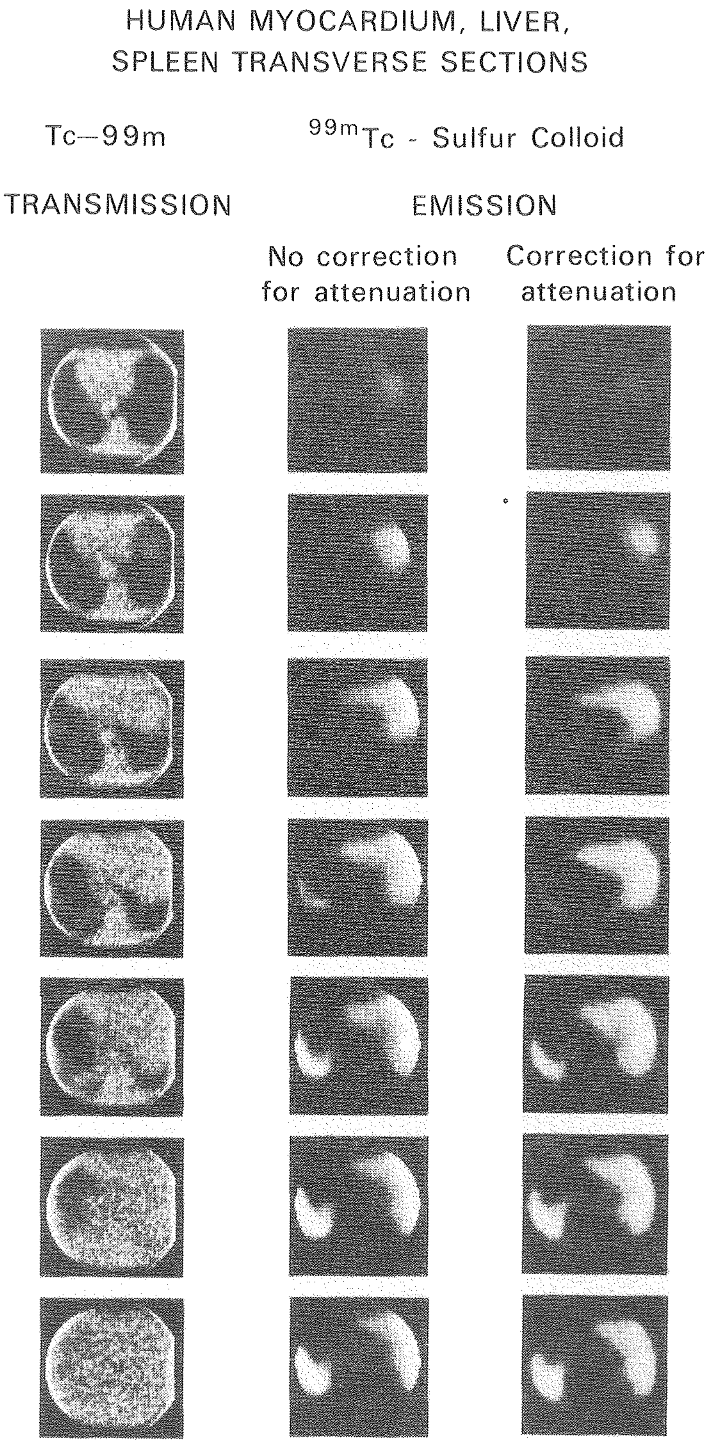

XBB 767-5951

Fig. 10. Accumulation of ^{99m}Tc-sulfur colloid in transverse sections of the liver and spleen are shown both with and without attenuation correction using the transmission reconstruction of the attenuation coefficients. In 72 projections over 360° the emission events in each transverse section totaled, from botton to top: 4.10×10^6, 4.58×10^6, 3.56×10^6, 2.69×10^6, 1.69×10^6, and 0.81×16^6 events. The incident number of photons per projection bin for the transmission study is, from the bottom to top: 1,556, 1,616, 1,611, 1,575, 1,534, 1,492, and 1,396.

7. Conclusions. This paper has developed a mathematical theory for single-photon emission computed tomography. The practical application of reconstructing projections attenuated by a variable attenuation coefficient was shown to involve iterative techniques of implementing a generalized inverse of the discrete attenuated Radon transform.

A major concern in the study of the attenuated Radon transform is how the magnitudes of the attenuation coefficients affect the rate of convergence for the iterative methods and how they amplify the statistical fluctuations of the measured data in the reconstructed image. Presently tracers are usually evaluated based on the specificity of the tracer to the target organ for the desired pathological study so that there is sufficient contrast between the target and surrounding tissue. They are also evaluated based on the camera system's ability to sufficiently collimate high-energy photons for isotopes such as Cs-129 or eliminate the Compton scattered photons by energy selection for a low-energy radionuclide such as ^{99m}Tc. However, simulations in [28] have shown that the rates of convergence for the iterative algorithms and the amplification of statistical errors for the iterative methods are a function of the magnitude of the attenuation coefficient. Therefore these tracers must also be evaluated based on the iterative algorithms' ability to accurately reconstruct the true concentration distribution in light of the increased statistical uncertainty for large attenuation experienced by low-energy radionuclides such as Tl-201.

The eigenfunctions and the spectrum of the operators $R_\mu R_\mu^*$ and $R_\mu^* R_\mu$ are an important mathematical construct because they give insight into how errors in the reconstructed image are propagated due to measurement errors. If weight functions in Theorems 8 and 10 are chosen so that the kernels K(4.14) and I(4.28) are L^2 kernels then there exist eigenfunctions for $R_\mu R_\mu^*$ and $R_\mu^* R_\mu$. However, explicit expressions for these eigenfunctions have not been developed for even the simplest case of constant attenuation. Only for the Radon transform have the eigenfunctions of $A_o^* A_o$ been expressed analytically [21],[49],[51],[52],[75]. The eigenfunctions of $A_o A_o^*$ have also been developed for various weight functions by Davison and Grünbaum [17]. Therefore research has been continuing to either analytically or numerically calculate the eigenfunctions and the spectrum for $R_\mu R_\mu^*$ and $R_\mu^* R_\mu$.

Inversion of the discrete attenuated Radon transform requires using iterative algorithms to reconstruct projection data attenuated by a variable attenuation coefficient. These algorithms converge with acceptable errors within 15 iterations for most radionuclides used in nuclear medicine. Simulations [28] have shown that the rate of convergence decreases as the magnitude of the attenuation coefficient increases above $\mu = 0.19\ \text{cm}^{-1}$ for a 30-cm diameter disk, so that at $\mu = 0.60\ \text{cm}^{-1}$ the result does not converge to an acceptable error criterion even after 30 iterations. This means that energies of photons emitted in tissue of less than 22 keV should not be used in single-photon ECT. The isotope of ^{131}Cs has a very low energy photon of 34.5 keV (x-rays of xenon) which has an attenuation coefficient of $0.27\ \text{cm}^{-1}$ in tissue. This isotope can be used for reconstructing transverse sections of the body in most areas where there is solid tissue; however, the presence of bone may yield artifacts due to the photoelectric absorption of calcium leading to an attenuation coefficient of $1.3\ \text{cm}^{-1}$. Isotopes of Tl-201 (73-80 keV, $\mu = 0.18\ \text{cm}^{-1}$), Tc-99m (140 keV, $\mu = 0.15\ \text{cm}^{-1}$), Se-75 (136 keV, $\mu = 0.15\ \text{cm}^{-1}$, 57%; 265 keV, $\mu = 0.125\ \text{cm}^{-1}$, 60%), and Cs-129 (375 keV, $\mu = 0.11\ \text{cm}^{-1}$, 48%) have been used for ECT with good contrast and spatial resolution.

Simulations [28] have also shown that the %RMS uncertainty increases with an increase in the attenuation coefficient. With the doses of radiopharmaceuticals presently used in nuclear medicine, the %RMS uncertainty in the reconstructed image ranges between 50% and 20%. Also errors in a transmission reconstruction used to determine the attenuation factors (5.7) induce additional errors in the emission reconstruction. This means that using Tc-99m as a brain scanning agent, the reconstructed %RMS uncertainty can be no better than 9.8%, even with infinite statistics, if the attenuation coefficients are determined from a transmission experiment with 1000 (4.2×10^6 total photons) incident photons per projection ray.

If the attenuation coefficient is constant, explicit inverse equations exist for a modified attenuated Radon transform [28] such that the back-projection of filtered projection algorithm [38] used in TCT applications extends nicely to single-photon ECT [28]. An important application of this method of attenuation compensation is the reconstruction of radionuclide distributions in the brain, where we find emission projection data can be reconstructed using an attenuation-dependent convolver or filter which reconstructs the transverse section reliably and requires little computer memory and very little computer time.

ACKNOWLEDGMENTS

The mathematical description of the attenuated Radon transform was formulated while performing patient and phantom studies under the direction of Professor Thomas Budinger. I am indebted to him for his direction and encouragement in this research. The many comments and suggestions of Dr. Ronald Huesman were invaluable in preparing this paper. The results for the single-angle projection operators were an extension of results for the Radon transform presented by Dr. Robert Marr in Professor Alberto Grünbaum's seminars on reconstruction tomography at the University of California, Berkeley, in the fall of 1978. I am grateful to both Dr. Marr and Professor Grünbaum for many helpful discussions. I also want to thank Professor Stanley Deans for the many comments and stimulating discussions concerning aspects of the attenuated Radon transform.

This research was supported in part by the Biology and Medicine Division of the Department of Energy (Contract W-7405-ENG-48), the National Cancer Institute (Contract YO1-CB-50304), and the National Heart, Lung and Blood Institute (Contract RO1-HL-21697).

REFERENCES

[1] H.O.Anger, The instruments of nuclear medicine: I, Hospital Practice, 7 (1972), pp.45-54.

[2] R.H.T.Bates and T.M.Peters, Towards improvements in tomography, New Zealand J. Sci., 14 (1971), pp.883-896.

[3] S.Bellini, M.Piacentini, C.Cafforio, and F.Rocca, Compensation of tissue absorption in emission tomography, IEEE Trans., ASSP-27(3) (1979), pp.213-218.

[4] ———, Design of a computerized emission tomographic system, Signal Processing, 1 (1979), pp.125-131.

[5] A.Ben-Israel and T.N.E.Greville, Generalized Inverses: Theory and Applications, John Wiley & Sons, New York, 1974 .

[6] T.L.Boullion and P.L.Odell, Generalized Inverse Matrices, John Wiley & Sons, New York, 1971 .

[7] R.N.Bracewell and A.C.Riddle, Inversion of fan-beam scans in radio astronomy, Astrophysics J., 150 (1967), pp.427-434.

[8] G.L.Brownell, C.A.Burnham, D.A.Chesler, J.A.Correia, J.E.Correll, B.Hoop,Jr., J.A.Parker, and R.Subramanyam, Transverse section imaging of radionuclide distributions in heart, lung, and brain, Reconstruction Tomography in Diagnostic Radiology and Nuclear Medicine, M.M.Ter-Pogossian et al., eds., University Park Press, Baltimore, MD, 1977 , pp.293-307.

[9] G.L.Brownell, J.A.Correia, and R.G.Zamenhof, Positron instrumentation, Recent Advances in Nuclear Medicine, Vol. 5, J.H.Lawrence and T.F.Budinger, eds., Grune & Stratton, New York, 1978 , pp.1-49.

[10] T.F.Budinger, J.L.Cahoon, S.E.Derenzo, G.T.Gullberg, B.R.Moyer, and Y.Yano, Three-dimensional imaging of the myocardium with radionuclides, Radiology, 125 (1977), pp.433-439.

[11] T.F.Budinger and G.T.Gullberg, Three-dimensional reconstruction in nuclear medicine emission imaging, IEEE Trans. Nucl. Sci., NS-21 (1974), pp.2-20.

[12] ———, Reconstruction by two-dimensional filtering of simple superposition transverse-section image, Technical Digest: Image Processing for 2-D and 3-D Reconstruction from Projections: Theory and Practice in Medicine and the Physical Sciences, August 4-7, 1975. Opt. Soc. Amer., Washington,D.C., 1975 .

[13] ———, Transverse section reconstruction of gamma-ray emitting radionuclides in patients, Reconstruction Tomography in Diagnostic Radiology and Nuclear Medicine, M.M.Ter-Pogossian et al., eds., University Park Press, Baltimore, MD, 1977 , pp.315-342.

[14] T.F.Budinger, G.T.Gullberg, and R.H.Huesman, Emission computed tomography, Image Reconstruction from Projections: Implementation and Application, G.T.Herman, ed., Springer-Verlag, New York, 1979 , pp.147-246.

[15] T.F.Budinger and F.D.Rollo, Physics and instrumentation, Progress in Cardiovascular Diseases, 20 (1977), pp.19-53.

[16] L.T.Chang, A method for attenuation correction in radionuclide computed tomography, IEEE Trans. Nucl. Sci., NS-25(2) (1978), pp.638-643.

[17] M.E.Davison and F.A.Grünbaum, Convolution algorithms for arbitrary projection angles, IEEE Trans. Nucl. Sci., NS-26(2) (1979), pp.2670-2673.

[18] S. E. Derenzo, T.F.Budinger, J.L.Cahoon, R.H.Huesman, and H.G.Jackson, High resolution computed tomography of positron emitters, IEEE Trans. Nucl. Sci., NS-24 (1977), pp.544-558.

[19] E.L.Dobson and H.B.Jones, The behavior of intravenously injected particulate material: its rate of disappearance from the blood stream as a measure of liver blood flow, Acta Med. Scand., 144, Suppl. 273 (1952), pp.1-71.

[20] N.Dunford and J.T.Schwartz, Linear Operators, Part II: Spectral Theory – Self-Adjoint Operators in Hilbert Space, Interscience Publishers, New York, 1963 .

[21] P.P.B.Eggermont, Three-dimensional image reconstruction by means of two-dimensional Radon inversion, Report No. T.H.-Report 75-WSK-04, Technological University, Eindhoven, Netherlands, 1975 .

[22] I.M.Gel'fand, M.I.Graev, and N.Ya.Vilenkin, Generalized Functions, Vol. 5: Integral Geometry and Representation Theory, Academic Press, New York, 1966 .

[23] S.Genna, S.C.Pang, and B.A.Burrows, Analysis of an arcuate gamma camera design for transaxial reconstruction, International Symposium on Medical Radionuclide Imaging, Vol. 1, IAEA, Vienna, 1976, pp.323-339.

[24] P.Gilbert, Iterative methods for the reconstruction of three-dimensional objects from projections, J. Theor. Biol., 36 (1972), pp.105-117.

[25] M.Goitein, Three-dimensional density reconstruction from a series of two-dimensional projections, Nucl. Instrum. Meth., 101 (1972), pp.509-518.

[26] R.Gordon, A tutorial on ART (algebraic reconstruction techniques), IEEE Trans. Nucl. Sci., NS-21 (1974), pp.78-93.

[27] R.Gordon, R.Bender, and G.T.Herman, Algebraic reconstruction techniques (ART) for three-dimensional electron microscopy and x-ray photography, J. Theor. Biol., 29 (1970), pp.471-481.

[28] G.T.Gullberg, The attenuated Radon transform: theory and application in medicine and biology, Ph.D. Thesis, University of California, Berkeley, CA (Lawrence Berkeley Laboratory Report LBL-7486, Berkeley, CA, 1979).

[29] ———, The reconstruction of fan-beam data by filtering the back-projection, Comp. Graphics & Image Processing, 10 (1979), pp.30-47.

[30] P.R.Halmos, Introduction to Hilbert Space and the Theory of Spectral Multiplicity, Chelsea, New York, 1951 .

[31] C.Hamaker and D.C.Solmon, The angles between the null spaces of x-rays, J. Math. Anal. & Appl., 62 (1978), pp.1-23.

[32] G.T.Herman and A.Lent, Iterative reconstruction algorithms, Comput. Biol. Med., 6 (1976), pp.273-294.

[33] G.T.Herman, A.Lent, and S.W.Rowland, ART: mathematics and applications (a report on the mathematical foundations and on the applicability to real data of the algebraic reconstruction

techniques), J. Theor. Biol., 42 (1973), pp.1-32.

[34] M.R.Hestenes and E.Stiefel, Methods of conjugate gradients for solving linear systems, J. Res. Nat. Bur. Standards, Sect. B., 49 (1952), pp.409-436.

[35] G.N.Hounsfield, Computerized transverse axial scanning (tomography): Part I. description of system, Br. J. Radiol., 46 (1973), pp.1016-1022.

[36] R.C.Hsieh and W.G.Wee, On methods of three-dimensional reconstruction from a set of radioisotope scintigrams, IEEE Trans., SMC-6(12) (1976), pp.854-862.

[37] J.G.Huebel and B.Lantz, A converging algebraic image reconstruction technique incorporating a generalized error model, Proceedings of Ninth Asilomar Conf. on Circuits, Systems, and Computers, November 3-5, 1975, (IEEE, 1975), pp.571-576.

[38] R.H.Huesman, G.T.Gullberg, W.L.Greenberg, and T.F.Budinger, RECLBL Library Users Manual — Donner Algorithms for Reconstruction Tomography, Technical Report PUB-214, Lawrence Berkeley Laboratory, Berkeley, CA, 1977 .

[39] R.J.Jaszczak, P.H.Murphy, D.Huard, and J.A.Burdine, Radionuclide emission computed tomography of the head with ^{99m}Tc and a scintillation camera, J. Nucl. Med., 18 (1977), pp.373-380.

[40] H.E.Johns and J.R.Cunningham, The Physics of Radiology, C. C. Thomas, Springfield, IL, 1974 .

[41] S.Kaczmarz, Angenaherte von Systemen linearer Gleichungen, Bull. Int. de l'Academie Polonaise des Sciences et des Lettres-Classe des Sciences Mathematiques et Naturelles, Serie A (1937), pp.355-357.

[42] W.J.Kammerer and M.Z.Nashed, On the convergence of the conjugate gradient method for singular linear operator equations, SIAM J. Numer. Anal., 9 (1972), pp.165-181.

[43] J.W.Keyes,Jr., N.Orlandea, W.J.Heetderks, P.F.Leonard, and W.L.Rogers, The Humongotron — a scintillation-camera transaxial tomograph, J. Nucl. Med., 18 (1977), pp.381-387.

[44] D.E.Kuhl and R.Q.Edwards, Image separation radioisotope scanning, Radiology, 80 (1963), pp.653-661.

[45] D.E.Kuhl, R.Q.Edwards, A.R.Ricci, R.J.Yacob, T.J.Mich, and A.Alavi, The Mark IV system for radionuclide computed tomography of the brain, Radiology, 121 (1976), pp.405-413.

[46] A.V.Lakshminarayanan and A.Lent, Methods of least squares and SIRT in reconstruction, J. Theor. Biol., 76 (1979), pp.267-295.

[47] B.F.Logan and L.A.Shepp, Optimal reconstruction of a function from its projections, Duke Math. J., 42 (1975), pp.645-659.

[48] D.Ludwig, The Radon transform on Euclidean space, Comm. Pure Appl. Math., 19 (1966), pp.49-81.

[49] C.D.Maldonado and H.N.Olson, New method for obtaining emission coefficients from emitted spectral intensities. Part II — asymmetrical sources, J. Opt. Soc. Amer., 56 (1966), pp.1305-1313.

[50] R.B.Marr, On the inversion of sampled Radon transforms, to appear as a Brookhaven National Laboratory Report, 1979.

[51] ———, On the reconstruction of a function on a circular domain from a sampling of its line integrals, J. Math. Anal. Appl., 45 (1974), pp.357-374.

[52] K.Miller, An optimal method for the x-ray reconstruction problem, Amer. Math. Soc. Not., 25 (1978), pp.A161-162.

[53] F.Natterer, On the inversion of the attenuated Radon transform, Report A78/17, Universitat des Saarlandes, Saarbrucken, 1978 .

[54] J.M.Ortega and W.C.Rheinboldt, Iterative Solution of Nonlinear Equations in Several Variables, Academic Press, New York, 1970 .

[55] I.G.Petrovskii, Lectures on the Theory of Integral Equations, Graylock Press, Rochester, NY, 1957 .

[56] M.E.Phelps, Emission computed tomography, Seminars in Nucl. Med., 7 (1977), pp.337-365.

[57] M.E.Phelps, E.J.Hoffman, Sung-Cheng Huan, and D.E.Kuhl, ECAT: a new computerized tomographic imaging system for positron-emitting radiopharmaceuticals, J. Nucl. Med., 19 (1978), pp.635-647.

[58] J.Radon, Über die Bestimmung von Funktionen durch ihre integralwerte längs gewisser Mannigfaltigkeiten, Berichte Saechsische Akademie der Wissenschaften, 69 (1917), pp.262-277.

[59] G.N.Ramachandran and A.V.Lakshminarayanan, Three-dimensional reconstruction from radiographs and electron micrographs: application of convolutions instead of Fourier transforms, Proc. Nat. Acad. Sci. U.S., 68 (1971), pp.2236-2240.

[60] W.T.Reid, Generalized inverses of differential and integral operators, Proceedings of the Symposium on Theory and Application of Generalized Inverses of Matrices, T.L.Boullion and P.L.Odell, eds., Texas Technological College Mathematics Series, No. 4, Lubbock, TX, 1968 , pp.1-25.

[61] A.Rosenfeld and A.C.Kak, Digital Picture Processing, Academic Press, New York, 1976 .

[62] L.A.Shepp and J.B.Kruskal, Computerized tomography: the new medical x-ray technology, Amer. Math. Monthly, 85(6) (1978), pp.420-439.

[63] L.A.Shepp and B.F.Logan, The Fourier reconstruction of a head section, IEEE Trans. Nucl. Sci., NS-21 (1974), pp.21-43.

[64] K.T.Smith, D.C.Solmon, and S.L.Wagner, Practical and mathematical aspects of the problem of reconstructing objects from radiographs, Bull. Amer. Math. Soc., 83(6) (1977), pp.1227-1270.

[65] F.Smithies, Integral Equations, Cambridge University Press, Cambridge, England, 1958 .

[66] H.F.Stoddart and H.A.Stoddart, A new development in single gamma transaxial tomography: Union Carbide focused collimator scanner, IEEE Trans. Nucl. Sci. NS-26(2) (1979), pp.2710-2712.

[67] G.Strang and G.J.Fix, An Analysis of the Finite Element Method , Prentice Hall, New York, 1973 .

[68] K.Tanabe, Projection method for solving a singular system of linear equations and its applications, Num. Math., 17 (1971), pp.203-214.

[69] M.M.Ter-Pogossian, Basic principles of computed axial tomography, Seminars in Nucl. Med., 7 (1977), pp.109-128.

[70] M.M.Ter-Pogossian, M.E.Phelps, E.J.Hoffman, and N.A.Mullani, A positron-emission transaxial tomograph for nuclear imaging (PETT), Radiology, 114 (1975), pp.89-98.

[71] O.J.Tretiak and P.Delaney, The exponential convolution algorithm for emission computed axial tomography, Review of Information Processing in Medical Imaging, Proceedings of 5th Internat'l. Conf., Vanderbilt University, June 27-July 1, 1977 , A.B.Brill and R.R.Price, eds., Oak Ridge National Laboratory Report ORNL/BCTIC-2, 1978 , pp.266-278.

[72] O.J.Tretiak and C.Metz, The exponential Radon transform, SIAM J. Appl. Math., in press, 1980.

[73] F.G.Tricomi, Integral Equations, Interscience Publishers, New York, 1965 .

[74] K.Yosida, Functional Analysis, 4th ed., Springer-Verlag, New York, 1974 .

[75] E.Zeitler, The reconstruction of objects from their projections, Optik, 39 (1974), pp.396-415.